Geophys. J. Int. (2002) **148,** 214–245

Active tectonics of the South Caspian Basin

James Jackson,[1] Keith Priestley,[1] Mark Allen[2] and Manuel Berberian[3]

[1] *University of Cambridge, Department of Earth Sciences, Bullard Laboratories, Madingley Road, Cambridge* CB3 OEZ, *UK. E-mails: jackson@esc.cam.ac.uk; priestley@esc.cam.ac.uk*

[2] *CASP, West Building,* 181A *Huntingdon Road, Cambridge* CB3 ODH, *UK. E-mail: mark.allen@casp.cam.ac.uk*

[3] *Najarian Associates, Suite E, One Industrial Way West, Eatontown,* NJ 07724-2255, *USA. E-mail: berberian@najarian.com*

Accepted 2001 August 14. Received 2001 July 24; in original form 2000 November 17

SUMMARY

We use observations of surface faulting, well-constrained earthquake focal mechanisms and centroid depths, and velocity structure determined by surface wave propagation and teleseismic receiver functions to investigate the present-day deformation and kinematics in and around the South Caspian Basin. The lack of earthquakes within the basin itself indicates that it behaves as a rigid block, though its sedimentary cover is deformed by numerous folds that are decoupled from its rigid basement by overpressured mud. The basin contains a sedimentary sequence almost 20 km thick above a relatively high-velocity basement that is thinner within the basin than on its margins. The basement beneath the basin could be either unusually thick oceanic crust or thinned, but relatively high-velocity, continental crust. The South Caspian Basin is surrounded by active earthquake belts on all sides. No earthquakes deeper than 30 km can be confirmed in the Kopeh Dag, Alborz and Talesh, which bound the NE, S and W sides of the basin. In contrast, earthquakes occur to depths of at least 80 km on the Apsheron–Balkhan sill, which bounds the N side of the basin and where no earthquakes can be confirmed that are shallower than 30 km. We interpret these deeper earthquakes to indicate the onset of subduction of the South Caspian Basin beneath the central Caspian, a process that appears to occur aseismically at shallow levels. Although oblique shortening is partitioned into pure strike-slip and pure thrust in many areas, conjugate right-lateral and left-lateral components in the Kopeh Dag and eastern Alborz suggest that the South Caspian Basin has a westward component of motion relative to both Eurasia and Iran. This motion enhances westward underthrusting of the basin beneath the Talesh mountains of Iran and Azerbaijan. We estimate the present motions of the South Caspian Basin to be $\sim$13–17 mm yr^{-1} to the SW relative to Iran (a maximum value) and $\sim$8–10 mm yr^{-1} to the NW or NNW relative to Eurasia. We suspect that these motions are all relatively recent, and may have begun only in the Pliocene (3–5 Ma). The South Caspian Basin will ultimately be destroyed by subduction or underthrusting and its present situation may represent an intermediate stage between that of the eastern Mediterranean and that of the seismically active slab beneath the Hindu Kush.

Key words: active tectonics, focal mechanisms, South Caspian Sea, velocity structure.

1 INTRODUCTION

This paper is concerned with the active tectonics and structure of the South Caspian Basin and its role in the collision between Arabia and Eurasia. On a map of earthquake epicentres (Fig. 1a), the southern Caspian Sea stands out as an aseismic block about 300×300 km^2 surrounded by belts of intense earthquake activity. Other similar aseismic blocks occur in the same region, such as the Dasht-e-Lut (L), central Iran (C) and NW Iran, and historical studies show that the seismicity within all of these blocks has been low for at least 1000 years (Ambraseys & Melville 1982). The implication is that these aseismic blocks are effectively rigid, and that the $\sim$30–35 mm yr^{-1} of N–S shortening between Arabia and Eurasia is absorbed in the active earthquake belts that surround them (Jackson & McKenzie 1984). However, the extent to which the active shortening in Iran is divided between the three major earthquake belts of the Zagros (Z), the Alborz–Kopeh Dag (A-K) and the Apsheron–Balkhan sill (the band that crosses the Caspian in Fig. 1a) is unknown and there are not yet sufficient GPS measurements in

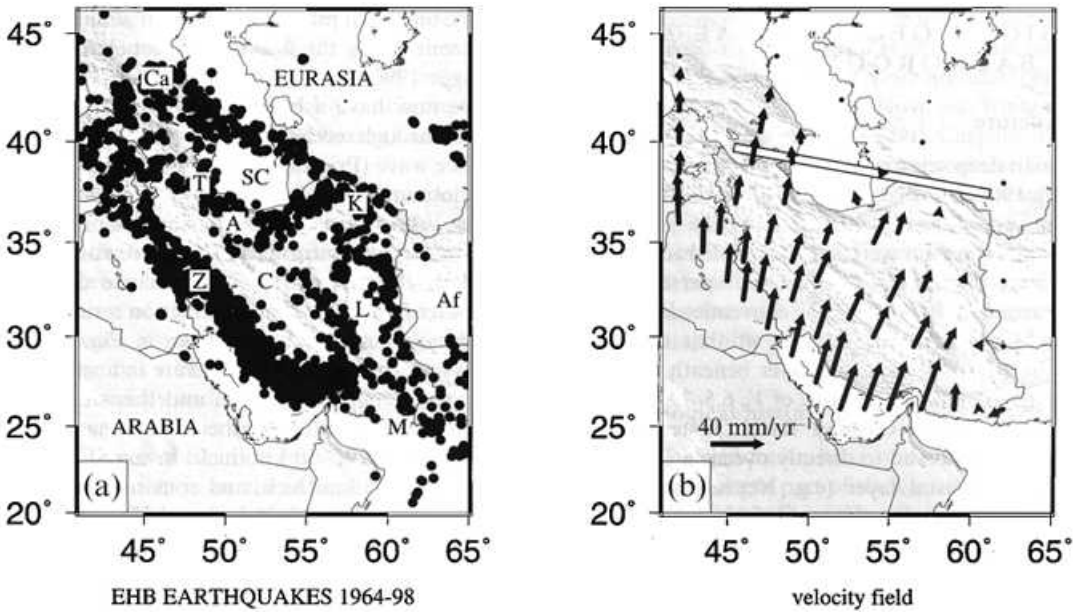

Figure 1. (a) Seismicity of Iran 1964–98, from the catalogue of Engdahl *et al.* (1998). The Zagros is marked by Z, the Alborz by A, the Kopeh Dagh by K, the relatively aseismic central Iran block by C, the Lut block by L, the Greater Caucasus by Ca, the Talesh by T, the Makran by M and Afghanistan by Af. (b) A velocity field showing how the NNE motion of Arabia relative to Asia is absorbed in Iran. The distribution of velocities within Iran is estimated from the spatial variation in the style of strain rates indicated by earthquakes (from Jackson *et al.* 1995). The white bar shows the line of the cross-section in Fig. 2.

Iran to determine it. A major issue is thus the current motion of the southern Caspian relative to central Iran in the south and Eurasia in the north.

At the longitude of the Caspian Sea the effects of the Arabia–Eurasia collision are contained between the rigid edges on the SW side of the Zagros mountains (the Arabian shield), the NE side of the Kopeh Dag and Caucasus (the Turan–Turkmen shield), and along the abrupt cut-off in seismicity following the Iran–Afghanistan border at 61°E. Jackson *et al.* (1995) showed that this roughly triangular shape of the deforming region is likely to be a major influence on the velocity field and the distribution of strain rates within Iran. In the same way, the relative motion of the South Caspian Basin is expected to influence strongly the deformation in the belts that surround it. Fig 1(b) shows a velocity field for Iran calculated by Jackson *et al.* (1995) using as constraints the overall Arabia–Eurasia plate motion and the distribution of strain rate orientations in Iran seen in earthquakes. They assumed that the South Caspian Basin was a relatively rigid block with little motion relative to Eurasia. In their scheme the southern Caspian is effectively a salient projecting into Iran and, as a result, we would expect right-lateral motion on its western margin (the Talesh) and left-lateral motion on its eastern margin (where the Alborz meets the Kopeh Dag). One motivation for this study is to test such predictions and use the deformation on the margins of the South Caspian Basin to estimate its motion.

The South Caspian Basin is of more than just regional or local interest. It differs from the other aseismic blocks in Iran in that it is very low, with much of it 500–1000 m below sea level, and for many years has been suspected of having an oceanic origin. In this respect it resembles the Black Sea (e.g. Okay *et al.* 1994) and the eastern Mediterranean (de Voogd *et al.* 1992), both of which are also thought to be oceanic remnants now caught up in continental collision zones. The role played by such basins in collisions, and their ultimate fates, is therefore of general interest in tectonics, and we will seek clues to these questions in the active deformation of the Caspian region today.

Finally, the South Caspian Basin is of intense commercial interest because of its prodigious hydrocarbon reserves, many of which are associated with very young (Plio-Quaternary) structures (e.g. Devlin *et al.* 1999). Some of these structures are closely connected with basement faults that move in earthquakes, while others are not. By providing a description of the basement-controlled seismogenic faulting in and around the southern Caspian, this study also aims to provide a framework for the interpretation of the structures of interest in hydrocarbon production.

The last overview of the active tectonics and earthquakes in this region was by Priestley *et al.* (1994). Since then we have gained a much better idea of the velocity structure of the region (Mangino & Priestley 1998; Priestley & Patton 2001), many more well-determined earthquake focal mechanisms and depths, and a better idea of the probable regional velocity field and its controls (Fig. 1b). An important conclusion of this paper is that the simple patterns of earthquake mechanisms that we see, and which hold the key to the tectonics of the South Caspian region, are not clear in the routinely reported earthquake bulletin data, mainly because of errors in focal depths. Those patterns are, however, clear when the focal mechanisms and depths have been improved by long-period waveform modelling. After an overview of the tectonic and geophysical background, we discuss the active faulting in the earthquakes surrounding the South Caspian Basin before returning to the major questions of how the basin is moving relative to Eurasia and Iran, how that motion is expressed in the deformation in its surrounding orogenic belts, and the role and ultimate fate of the basin within the Arabia–Eurasia collision.

2 GEOLOGICAL, GEOPHYSICAL AND TECTONIC BACKGROUND

2.1 Crustal structure

The earliest Russian deep seismic sounding (DSS) experiments in the 1950s and 1960s showed that the crust of the South Caspian Basin is very different from that of the surrounding region. However, the data were seldom published and the velocity models were more intricate than the sparse seismograph coverage warranted. In terms of the conventional Russian characterization of the continental crust at that time, the 'granitic' crust, the V_p 5.8–6.5 km s^{-1} layer beneath the sediments and above the 'basaltic' lower crust of V_p 6.5–7.8 km s^{-1}, is missing within the South Caspian Basin. Instead, thick (15–25 km) sediments appeared to directly overlie a 12–18 km thick 'basaltic' lower crustal layer (e.g. Neprochnov 1968). While some authors suggest that the 'granitic' layer is missing because of uplift, erosion and later subsidence (e.g. Rezanov & Chamo 1969; Shikalibeily & Gigoriants 1980), others speculate that the 'basaltic' layer in the South Caspian Basin is remnant oceanic crust, which is consistent with the efficient propagation of S_n waves and the blocking of L_g waves on paths across the basin (e.g. Kadinsky-Cade *et al.* 1981). Various origins have been suggested for such a remnant piece of ocean floor, including the isolation of part of a late Mesozoic or early Tertiary marginal ('backarc') basin (e.g. Berberian & King 1981; Berberian 1983; Zonenshain & Le Pichon 1986; Philip *et al.* 1989), a remnant of the Tethys ocean itself (Dercourt *et al.* 1986; Nadirov *et al.* 1997), or even a pull-apart basin on a major Cretaceous strike-slip zone along the line of the Kopeh Dag–Caucasus ranges (Şengör 1990).

We now have a better idea of the crustal structure in the region through receiver function (Mangino & Priestley 1998) and surface wave (Priestley & Patton 2001) analysis of broad-band seismograms recorded at new digital seismographs installed around the South Caspian Basin. Not only do these data provide new crustal information on the region, but they can also be used to check, calibrate and enhance our understanding of the older published seismic refraction results. A summary of the results of these studies is shown in Fig. 2. Receiver function analysis gives the crustal structure in a small region surrounding the seismograph station and this shows that the crust in Turkmenia east of the Apsheron–Balkhan sill and north of the Kopeh Dag is 45–50 km thick. In the SE part of the basin the crust is 30–35 km thick, and consists of a 10 km sedimentary section overlying a 15–20 km crystalline crust of V_p 5.8 km s^{-1}, which in turn overlies a thin lower crust. The crustal velocity structures determined from receiver function analysis in Turkmenia are consistent with the crustal structure seen in the older refraction literature for the same region. Receiver function analysis for data from the SW part of the South Caspian Basin shows that the crust consists of 13 km of sediments overlying a high-velocity (V_p 7.1 km s^{-1}) basement with a Moho at 33 km. Priestley & Patton (2001) inverted Rayleigh wave phase–velocity curves to obtain an average crust and upper mantle model for paths across the South Caspian Basin. Their results confirmed the presence of thick, low-velocity sediments over a crystalline

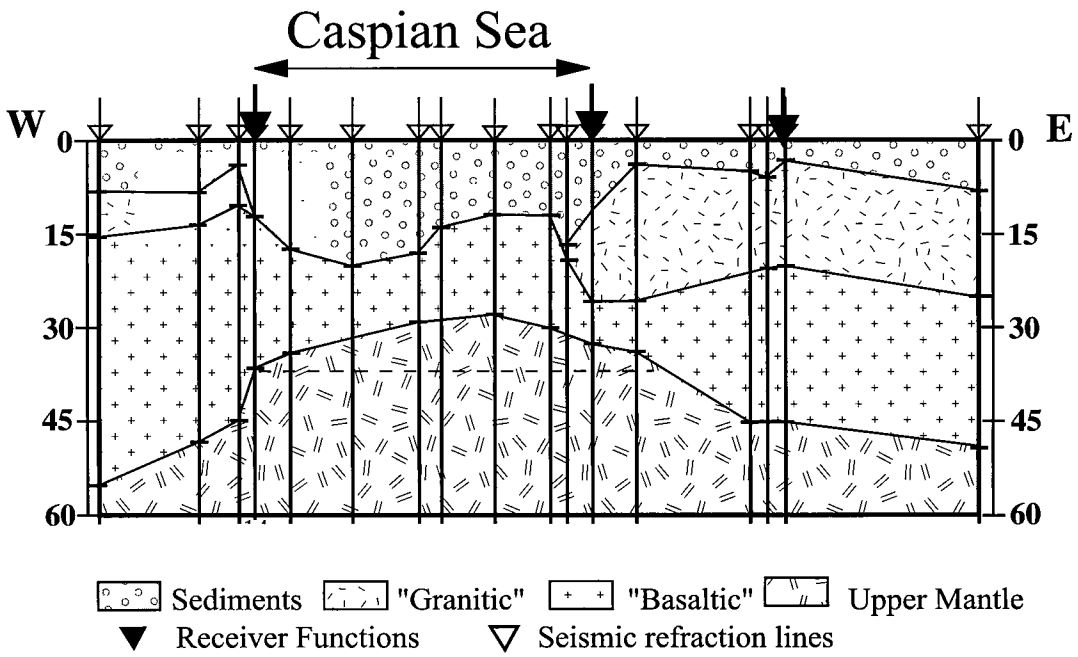

Figure 2. Crust and uppermost mantle cross-section between the Kura Basin to the west of the South Caspian Basin (~39.5°N, 46.0°E) and the Turkmenian lowlands and the Kopeh Dag mountains to the east (~37.5°N, 61.5°E): see Fig. 1(b) for location. The approximate extent of the South Caspian Basin is denoted by the double-headed horizontal arrow above the cross-section. The structure is summarized in terms of four generalized rock types: low-velocity sediments; the upper 'granitic' crust consisting of rocks with V_p 5.8–6.5 km s^{-1}; the lower 'basaltic' crust consisting of rocks with V_p 6.5–7.8 km s^{-1}; and the upper mantle. The vertical arrows at the top of the cross-section denote points where receiver function analysis (large solid arrows) or Russian refraction analysis (small open arrows), both from Mangino & Priestley (1998), provide a constraint on the crustal structure. The surface wave study of Priestley & Patton (2001) is for the path denoted by the double-headed arrow above the cross-section. The dashed line at 35 km depth beneath the basin denotes the approximate position of the Moho from the surface wave analysis.

basement 20–25 km thick, somewhat thicker than inferred from the older refraction studies. Beneath the crust, there is an upper mantle lid ~50 km thick with V_s 4.65–4.70 km s^{-1}. The S-wave velocity in the lid agrees well with the observed S_n velocity of ~4.70 km s^{-1} observed across the basin (Kadinsky-Cade *et al.* 1981).

The most significant features of the crustal model in Fig. 2 are: (1) a 20 km variation in the thickness of the sedimentary section across the basin; (2) the absence of a 'granitic' (V_p 5.8–6.5 km s^{-1}) layer beneath the central part of the basin; and (3) a thinning of the crust beneath the basin by 15–20 km compared with its margins. The Moho beneath the South Caspian Basin has a broad arch-like structure, with the crust thinning more rapidly under its western boundary (by 20 km over 100 km) than under its eastern boundary (20 km over 400 km). The only receiver function result to the south of the Caspian in northern Iran is in the Alborz Mountains, showing that the crust is ~35 km thick with a structure typical of the continents (M. Tatar, private communication, 2000) and confirming earlier suggestions that the Alborz has no significant root (Deghani & Makris 1984). North of the Apsheron sill the crust appears to be relatively 'normal' continental in character and ~45–50 km thick (Mangino & Priestley 1998).

These new results are compatible with the previous suggestions that the South Caspian Basin is an oceanic remnant, with an abrupt western margin and a more gradual (perhaps originally extended) margin on the east. However, while the velocities of the crystalline basement in the south Caspian, and its S_n and L_g propagation characteristics, are appropriate for oceanic crust, the thickness of the layer (15–18 km) indicates that if it is oceanic it is unusually thick, since normal oceanic crust has an almost uniform thickness of about 7 km (White *et al.* 1992). An alternative possibility is that the south Caspian is thinned continental crust with unusually high basement velocities, but this is incompatible with the observed S_n and L_g propagation.

2.2 Geological history

The principal mountain belts surrounding the South Caspian Basin are the eastern part of the Greater Caucasus, the Talesh, Alborz and Kopeh Dag (Fig. 3). All involve major crustal shortening in response to the Arabia–Eurasia collision. Initial contact of the northern promontory of Arabia with other continental material, which may or may not have been part of Eurasia, appears to have begun as early as 45 Ma, suggested by thrusting of this age in eastern Anatolia (Hempton 1987) and

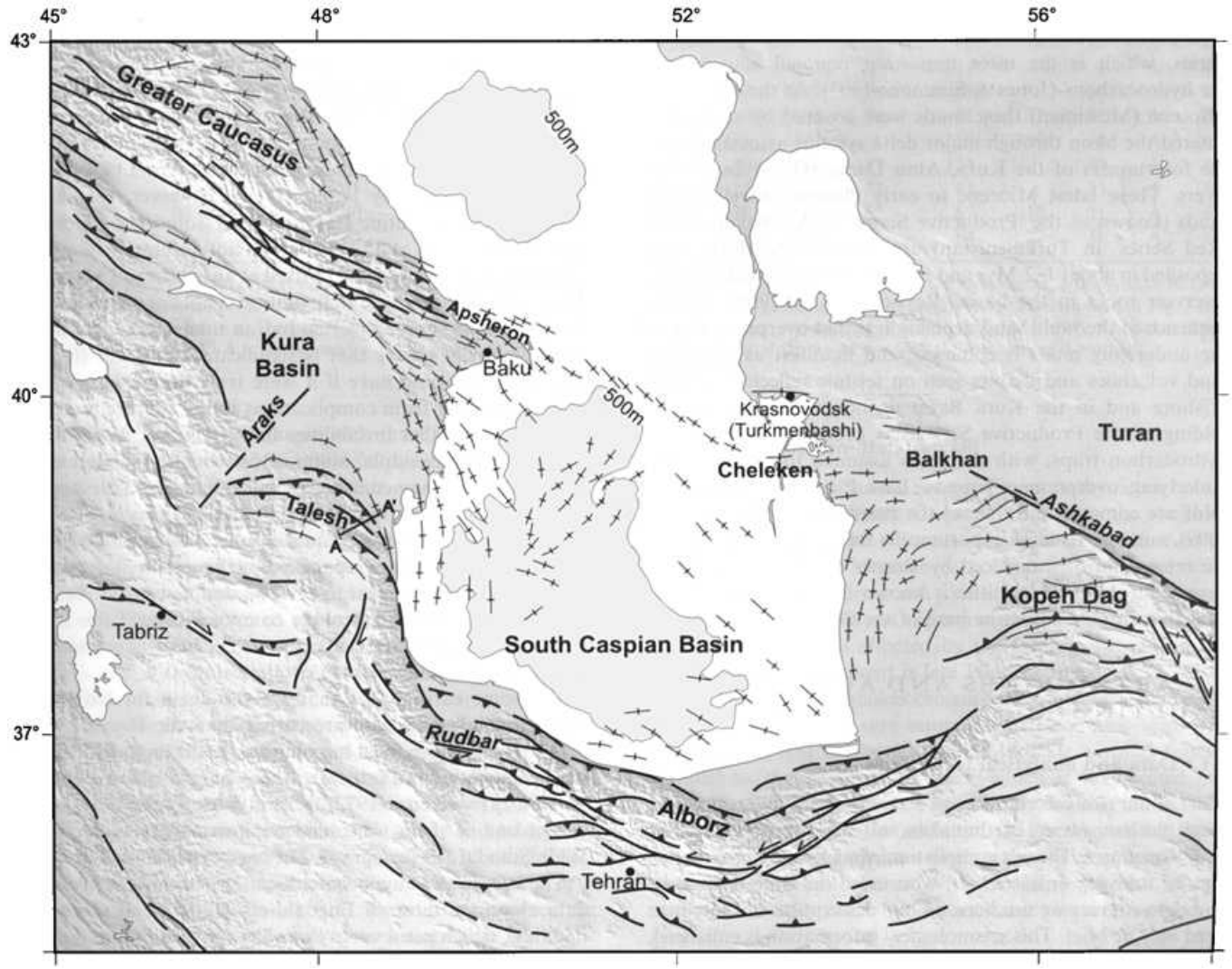

Figure 3. Summary structural map of the South Caspian Basin, adapted from Hinds *et al.* (2001).

by the local appearance of poorly dated, but probably Eocene, terrestrial clastic sediments in the same region (Buday 1980). However, much of the broader collision zone did not start to deform until the mid-Miocene or later (Dewey *et al.* 1986) and, in particular, major deformation in the Simple Folded Belt of the Zagros mountains appears not to have begun until the Pliocene, ~5 Myr or less ago (Falcon 1974). This time lag may be because the main Eurasia landmass was separated from Arabia by several smaller continental blocks, now preserved within central Iran (Berberian & King 1981). Deep-water marine sediments among the coloured melange zones of NE Iran indicate that the final closure of minor ocean basins separating the various Iranian tectonic blocks may not have occurred until the mid-Tertiary (McCall 1996). We suspect that only when these central Iranian blocks had finally accreted to each other did the Arabia–Eurasia convergence really affect the Simple Folded Belt of the Zagros in the south and the South Caspian Basin in the north (see also Axen *et al.* 2001).

The South Caspian Basin itself contains some of the thickest sediment accumulations known on Earth. Since it is surrounded on all sides by mountain belts, these sediments have mostly accumulated in a post-Oligocene foreland basin setting, perhaps superimposed on sediments from an earlier (sea-floor?) basin-forming event responsible for the formation of the underlying crust itself. Of particular interest is a thick mud-prone sequence of Oligo-Miocene age called the Maykop Series, which is the most important regional source rock for hydrocarbons (Jones & Simmons 1997). At the end of the Miocene (Messinian) these muds were covered by sands that entered the basin through major delta systems associated with the forerunners of the Kura, Amu Darya (Oxus) and Volga rivers. These latest Miocene to early Pliocene fluvial–deltaic sands (known as the 'Productive Series' in Azerbaijan or the 'Red Series' in Turkmenistan) are up to 5 km thick, were deposited in about 1–2 Myr and form the principal hydrocarbon reservoir rocks in the basin (Reynolds *et al.* 1998). A consequence of the rapid sand deposition is that overpressuring of the underlying muds is common, and manifest as abundant mud volcanoes and diapirs seen on seismic reflection profiles offshore and in the Kura Basin onshore. Post-depositional folding of the Productive Series has produced many of the hydrocarbon traps, with the folds assumed to detach in the underlying overpressured muds. Late Pliocene and younger folds are common throughout the basin (Fig. 3; Devlin *et al.* 1999), and one issue of importance is the extent to which they are related to, or influenced by, deeper active faulting in the basement, about which little is known from industry seismic data that rarely images the base of the Oligo-Miocene muds.

3 EARTHQUAKES AND ACTIVE FAULTING

3.1 Data and analytical techniques

Most of our new information on active faulting comes from the focal mechanisms of earthquakes and from some co-seismic surface ruptures. The last compilation of such data in this region was by Priestley *et al.* (1994), who used the same techniques and data sources we use here, so our description of these here need only be brief. This seismological information is enhanced, where available, by observations of Quaternary faults and folds, though their description is not a major focus of this paper.

The best-determined earthquake focal mechanisms and depths are those based on an analysis of long-period teleseismic *P* and *SH* waveforms of events larger than about M_w 5.4 (Table 1). We have increased from 17 to 34 the number of earthquakes we have analysed in this way since Priestley *et al.* (1994). We took digital broad-band records from stations of the GDSN in the epicentral range 30–90° and convolved them with a filter that reproduces the bandwidth of the WWSSN 15–100 s long-period instruments. We then used the MT5 version (Zwick *et al.* 1994) of McCaffrey & Abers' (1988) and McCaffrey *et al.*'s (1991) algorithm, which inverts the *P* and *SH* waveform data to obtain the strike, dip, rake, centroid depth, seismic moment and the source time function, which is parametrized by a series of isosceles triangle elements of half-duration τ s. We always constrained the source to be a double-couple. The method and approach we used, and the way in which we estimated uncertainties in source parameters, are described in detail elsewhere (e.g. Nábělek 1984; McCaffrey & Nábělek 1987; Molnar & Lyon-Caen 1989; Priestley *et al.* 1994) and are too routine to justify repetition here. Details of the inversions and the waveforms used for the new earthquakes in Table 1 are given in the Appendix. For most of these events the centroid depth is constrained to within $\pm$4 km, the strike and rake to within $\pm$15–20° and the dip to within 5°.

Where we were unable to analyse the waveforms ourselves (usually because they were too small) we could make use of the Harvard Centroid Moment Tensor (CMT) catalogue (Harvard 2000), which routinely publishes moment tensor analyses for earthquakes larger than about M_w 5.0. The number of such additional events we could use has increased from 11 to 40 since the study of Priestley *et al.* (1994). However, for shallow earthquakes the routine Harvard CMT solutions, which low-pass filter the data at 45 s period, do not accurately resolve the centroid depth, which is often fixed at an arbitrary 15 or 33 km. Moreover, because the CMT solution is not constrained to be a double-couple source, it often has an intermediate eigenvalue to the moment tensor that is significantly different from the zero value it would have if it were truly double-couple. This may arise either from complications in the rupture process or from noise or other instabilities in the solution. In such cases the 'best-double-couple' solution (in which the intermediate eigenvalue is assigned a zero value and its corresponding eigenvector taken to be the B or null axis) may not be truly representative of the earthquake source as a whole. In our discussion we therefore separate those simple, well-determined CMT sources that appear to be good double-couples (i.e. more than 70 per cent double-couple component: see Table 2 for a definition), from those that appear to have a greater non-double-couple component.

For some earthquakes that are too small for long-period waveform inversion and are earlier than the Harvard CMT catalogue, we have focal mechanisms based on long-period *P*-wave first motions (Table 3). These have all been published previously (McKenzie 1972; Jackson & McKenzie 1984) and all except one of them were read on instruments of the World Wide Standard Seismograph Network (WWSSN) after 1963.

The best routine hypocentre locations based on arrival time data alone are those of Engdahl *et al.* (1998 and subsequent updates), which use a variety of phases in addition to direct *P*, and, in particular, include surface reflections to improve depth control. Maggi *et al.* (2000b) compared the depths from

Table 1. Earthquake source parameters determined by body wave modelling.

Date			Time	Lat.	Long.	M_w	s1	d1	r1	s2	d2	r2	sv	z	R	Fig.
1962	9	1	1920	35.70	49.80	6.98	311	42	113	100	52	70	41	10	P	4
1969	1	3	0316	37.11	57.81	5.45	304	40	84	132	49	95	34	7	P	4
1970	7	30	0052	37.85	55.92	6.35	293	56	−150	185	65	−37	23	11	P	4
1971	2	14	1627	36.64	55.72	5.67	336	39	93	152	51	87	66	11	P	4
1972	12	I	1139	35.45	57.92	5.38	156	65	−176	64	87	−25		8	P	4
1978	11	4	1522	37.71	48.97	6.12	141	12	65	346	79	95	76	21	P	4
1979	12	9	0912	35.15	56.87	5.55	325	36	99	133	54	83		9	B	4
1980	5	4	1835	38.07	49.04	6.34	27	6	−63	181	84	−93	91	15	P	4
1981	8	4	1835	38.20	49.43	5.52	154	35	32	36	72	120	126	20	P	4
1983	7	22	0241	36.93	49.24	5.45	120	35	83	308	55	94	30	10	P	4
1984	2	22	0544	39.47	54.05	5.74	106	60	174	199	84	30	289	27	P	4
1985	10	29	1423	36.79	54.84	6.16	106	30	126	246	65	71	336	13	P	4
1986	3	6	0005	40.38	51.62	6.38	50	5	−158	299	88	−85		31	P	6
1987	9	7	1132	39.47	54.81	5.51	305	10	103	111	80	87	31	30	P	4,6
1989	9	16	0205	40.35	51.57	6.49	80	26	−135	308	71	−70		31	P	6
1989	9	17	0053	40.23	51.81	6.16	127	44	−66	277	49	−111		35	P	6
1990	6	20	2100	36.96	49.33	7.30	301	82	5	210	85	171	120	12	C	4
1990	6	21	0902	36.61	49.81	5.59	170	28	81	1	62	95		10	A	4
1991	11	28	1720	36.84	49.61	5.66	185	44	101	350	47	80		8	A	4
1993	8	31	0655	41.87	49.47	5.13	221	37	37	100	69	121		76	A	6
1994	7	1	1012	40.19	53.35	5.58	259	24	78	92	67	95		42	A	6
1994	7	1	1950	40.20	53.37	5.11	251	20	69	94	71	97		41	A	6
1995	10	29	0627	39.56	51.90	5.32	49	77	−166	316	76	−13		61	A	6
1997	2	4	0953	37.39	57.33	5.40	338	67	150	80	63	26	350	13	A	4
1997	2	4	1037	37.39	57.35	6.44	326	75	173	58	83	15	328	8	A	4
1997	2	28	1257	38.10	47.79	6.00	183	81	−1	273	89	−171		9	A	4
1997	5	7	1616	40.33	51.63	5.20	287	40	−115	138	53	−69		50	A	6
1998	7	9	1419	38.71	48.50	5.69	72	8	0	342	90	98	72	27	A	6
2000	8	22	1655	38.07	57.19	5.59	133	69	171	227	81	−150	317	4	A	4
2000	11	25	1809	40.29	50.06	6.18	317	76	−80	101	17	−124		40	A	6
2000	11	25	1810	40.31	50.09	6.08	313	70	−115	187	32	−41		33	A	6
2000	12	06	1711	39.40	55.04	6.86	322	36	127	100	62	67	10	31	A	6
2001	6	10	0152	39.83	53.89	5.31	335	40	125	112	58	64	22	31	A	6

Epicentres are from Engdahl *et al.* (1998) and their updated catalogue. M_w is the moment-magnitude, calculated from the formula: $M_w = (\log_{10} M_0 - 16.1)/1.5$, where M_0 is the moment in N m. The strikes, dips and rakes of the two nodal planes are s1, d1, r1 and s2, d2 r2. The slip vector azimuth used in Fig. 8 is sv. The centroid depth in km is z. The penultimate column refers to the work in which the inversion is published: P is Priestley *et al.* (1994), B is Baker (1993), C is Campos *et al.* (1994); A is the Appendix of this paper. In the final column is the number of the figure in which the mechanism is plotted.

Engdahl *et al.*'s (EHB) catalogue with those determined from waveforms, and found that for well-recorded events with depths of ~60 km or greater the agreement was generally good, probably because the surface reflections are well separated from direct phases and more reliably identified by station operators. However, the EHB catalogue can be in error by up to 30 km for shallower earthquakes. Nonetheless, the EHB catalogue is better than the catalogues of either the International Seismological Centre (ISC) or the United States Geological Survey (USGS), and is complete above about M_w 5.2 in the interval 1964–1998.

Thus for shallow earthquakes we show two maps. The 'better' solutions are shown in Fig. 4, containing (in hierarchy, to avoid two solutions for any earthquake) those based on waveform analysis, additional CMT solutions with >70 per cent double-couple component and $M_w \geq 5.3$, and additional first-motion solutions after 1963. Fig. 5 contains all other CMT solutions (irrespective of double-couple component and M_w) and one first-motion solution in 1957. By referring between the two figures the reader can see all the solutions that are available, with some idea of relative quality. The earthquakes known (or suspected) to be at 30 km or deeper are shown in Fig. 6.

3.2 The Apsheron–Balkhan sill

The Apsheron–Balkhan sill is a prominent bathymetric feature separating the deep South Caspian Basin from the shallower northern Caspian. The sill coincides with an anticline in the sediments of the late Miocene–early Pliocene productive series, but its deeper structure is not well imaged on industry seismic reflection profiles. Only at the top of the Productive Series are sediment thicknesses affected by the folding, suggesting that the anticline development is late Pliocene in age.

The band of earthquakes crossing the central Caspian along the line of the sill is very anomalous. It contains some substantial ($M_w > 6$) earthquakes that indicate normal faulting parallel to the strike of the belt, which is unexpected in a collision zone setting, as well as as thrust-faulting earthquakes with the same strike. In addition, as Priestley *et al.* (1994) demonstrated, some of these earthquakes have unusually deep centroids, of 30 km or more. With the additional data since the study of Priestley *et al.* (1994), a clearer pattern has emerged (Fig. 6).

As far as focal depths are concerned, all of the 14 events in the Apsheron–Balkhan sill zone where the source parameters

Table 2. Best-double-couple Harvard CMT solutions.

Date			Time	Lat.	Long.	M_w	s1	d1	r1	s2	d2	r2	sv	γ	z	Fig.
1978	5	26	1343	41.96	46.55	5.5	280	17	71	119	73	95	29	90	23	4
1979	10	1	0736	40.08	51.91	5.0	304	20	−63	95	72	−99		76	35/48	6
1980	7	22	0517	37.19	50.20	5.5	135	20	95	309	70	88	39	50	29	5
1980	12	3	0426	37.08	50.38	5.3	160	52	136	280	56	47		69	16	5
1981	2	23	0406	41.79	45.98	5.2	333	35	145	92	70	60	2	93	33f	5
1981	7	21	0445	39.47	53.26	5.3	290	87	−2	20	88	−176		74	42/38	6
1981	7	23	0005	37.14	45.23	5.8	170	27	−73	330	63	−98		71	15	4
1981	11	19	1410	40.73	49.19	5.1	34	68	162	130	73	23		94	33f	5
1983	3	25	1157	35.95	52.26	5.4	280	68	4	188	85	157		93	33f	4,7b
1983	3	26	0407	36.13	52.29	5.3	104	61	17	5	75	149	95	60	10	5,7b
1983	8	20	0546	40.74	51.79	5.1	164	34	−34	283	71	−119		39	39/49	6
1985	7	4	0508	42.29	45.94	5.4	192	15	14	87	86	104	357	77	15f	4
1986	6	11	2015	40.43	51.71	5.2	291	43	−123	152	55	−63		89	50/51	6
1987	4	10	0643	37.13	57.68	5.1	292	45	29	179	69	130	22	99	15f	5
1987	12	19	0827	40.74	52.11	5.0	322	36	109	117	56	76		89	33f/73	6
1988	5	3	0915	42.40	47.54	5.3	126	16	89	307	74	90	37	83	15f	4
1988	8	22	2123	35.23	52.34	5.3	317	75	−175	225	85	−15		70	15f	4
1988	8	23	0530	35.38	52.31	5.1	348	31	−41	114	69	−115		71	15f	5
1990	1	20	0127	35.82	52.92	5.9	357	66	172	90	82	24	87	72	33f*	4,7b
1990	6	24	0945	36.82	49.42	5.3	234	69	−163	137	74	−21	144	34	15f	5,7a
1990	7	6	1934	36.82	49.31	5.3	94	37	6	359	86	126		78	15f	4,7a
1992	9	22	1405	36.33	52.70	5.0	268	44	75	108	47	104	358	97	33f	5,7b
1992	10	23	2319	42.50	45.07	6.4	302	13	144	67	82	79	337	93	15f	4
1995	10	15	0656	37.06	49.53	5.1	65	49	178	157	88	41		43	15f	5,7a
1996	1	3	0842	39.03	48.72	5.3	261	5	125	45	85	86	135	87	15f	4
1996	2	25	1614	35.65	57.07	5.4	82	77	10	349	80	166		92	33f	4
1996	2	25	1742	35.65	57.05	5.3	257	79	5	166	85	168		64	33f	5
1997	2	5	0753	37.63	57.59	5.2	187	78	−178	96	88	−12		68	15f	5
1997	3	2	1829	37.86	47.87	5.3	200	40	1	108	88	130		62	15f	5
1997	11	27	1734	41.85	45.33	5.2	103	39	122	244	57	66		93	41	6
1998	8	4	1141	37.34	57.26	5.3	252	84	−6	342	84	−173	342	85	15f	4
1999	1	15	1914	35.35	45.16	5.1	127	29	85	312	61	92	42	76	33f	5
1999	6	4	0912	40.80	47.45	5.4	193	40	68	40	53	107	103	80	32	4
1999	11	19	0440	37.34	54.40	5.4	57	34	51	281	64	113	11	100	29	4
1999	11	26	0427	36.92	54.90	5.3	106	22	58	319	71	102	49	58	17	5
2000	1	26	2300	40.02	52.90	5.3	98	65	25	357	67	152		69	65†	6
2000	3	21	1407	39.95	48.23	5.1	240	45	−145	123	66	−50		49	54	6
2000	8	16	1253	36.72	54.36	4.9	240	34	78	74	57	98	330	76	15f	5
2000	9	19	1519	38.30	57.48	5.1	40	78	−3	131	87	−168	310	91	35	6
2001	1	7	0649	40.17	50.14	5.2	359	22	−159	249	82	−70		77	48	6

This table shows the Harvard CMT solutions used in Figs 4–6, but omits those earthquakes where the source parameters are already listed in Table 1. M_w is the moment-magnitude, calculated as in Table 1. The strikes, dips and rakes of the two nodal planes are s1, d1, r1 and s2, d2 r2. The slip vector azimuth used in Fig. 8 is sv. γ is the percentage double-couple component, defined from the absolute value of the intermediate eigenvalue relative to the average of the other two, normalized so that a pure double-couple source (with eigenvalues −1, 0, +1) is 100 per cent, while a linear vector dipole (e.g. −0.5, −0.5, +1.0) is 0 per cent. Thus $\gamma = 100 - \{1 - [(2|\lambda_2| \times 1.5)/(|\lambda_1| + |\lambda_3|)]\}$, but other definitions are possible. The centroid depth reported by Harvard is z (km), followed by a second depth from Engdahl *et al.* (1998) if one is available. Note that depths of 15 and 33 km are held fixed in the Harvard inversion (and marked f). The depths for 1990.1.20 (*) and 2000.1.26 (†) have been confirmed as ~13 and 55 km by waveform modelling (see the Appendix). In the final column is the number of the figure in which the mechanism is plotted.

can be constrained by waveform modelling have centroid depths of ≥30 km, with the deepest reaching 75 km. There are also CMT solutions for an additional seven earthquakes that were too small for us to model their long-period waveforms, all of which have depths in the EHB or CMT catalogue of ≥38 km. These EHB and CMT depths agree well with those of nearby events the depths of which are better determined from waveforms. In addition, the EHB catalogue lists several other earthquakes in this band of seismicity with depths ≥60 km and only a few of that depth that are outside. There is one small earthquake (2000.03.21, M_w 5.1) in the Kura Basin with a CMT depth estimate of 54 km (Fig. 6), but we are not sure whether that depth is correct. The ISC catalogue lists numerous events on the Apsheron–Balkhan sill that are apparently at depths <30 km but, in contrast to the EHB catalogue (which is for events of $\gtrsim M_w$5.2), these are all small and their depths are unlikely to be reliable. Outside the Apsheron–Balkhan sill zone there are only two CMT depths that are claimed to be ≥35 km (Fig. 6), whereas all the well-determined centroid depths are <30 km (Fig. 4) and mostly less than 15 km: only in the Talesh are some as deep as 20–26 km.

The pattern of depths is thus relatively simple: only in the Apsheron–Balkhan sill zone is there unequivocal evidence for earthquakes deeper than 30 km, and in this place they extend at

Table 3. First-motion fault plane solutions.

Date			Time	Lat.	Long.	M_s	s1	d1	r1	s2	d2	r2	sv	R	Fig.
1957	7	2	0042	36.05	52.45	6.8	104	44	80	297	46	99	27	M	5
1966	4	20	1642	41.73	48.18	5.4	131	28	90	311	61	90	41	M	4
1970	5	14	1812	42.95	46.90	6.6	130	26	90	310	64	90	40	J	4
1970	10	25	1122	36.75	45.17	5.5	319	49	−154	211	70	−43		J	4
1971	12	20	0141	41.21	48.47	5.2	99	0	89	280	89	90	10	J	4
1972	12	1	1139	35.45	57.92	5.2	82	80	10	350	80	169		J	4
1973	8	2	1956	37.41	56.51	5.3	48	89	0	318	90	179		J	4
1974	3	7	1136	37.70	55.94	5.1	23	89	0	293	90	179	23	J	4
1974	8	4	1506	42.39	45.98	5.4	300	45	90	120	45	90	30	J	4
1976	2	3	1640	39.95	48.40	5.2	297	72	−175	206	86	−17		J	4

First-motion fault plane solutions used in Figs 4 and 5. Epicentres are from Engdahl *et al.* (1998). M_s is surface wave magnitude. The strikes, dips and rakes of the two nodal planes are s1, d1, r1 and s2, d2, r2. The slip vector azimuth used in Fig. 8 is sv. The penultimate column refers to the work in which the first-motion polarities are published. M is McKenzie (1972); J is Jackson & McKenzie (1984). In the last column is the number of the figure in which the mechanism is plotted.

least as deep as 75 km. Furthermore, there is very little evidence for any earthquakes shallower than 30 km in the offshore part of this trans-Caspian sill zone (Fig. 4). The best is from a second (thrust) subevent 13 s after the main (normal) shock of 1986.03.06. Priestley *et al.* (1994) studied this earthquake in detail and concluded that while the first subevent had a centroid of ~31 km depth, the second was much shallower, at 13 ± 4 km. The only other evidence for shallow seismicity on the sill is from two earthquakes listed as <30 km in the EHB catalogue (one of which is the earthquake of 1986.03.06, above, now known from waveform modelling to be at ~31 km).

The pattern of focal mechanisms on the sill is also relatively simple (Fig. 6). In the offshore area most indicate normal faulting parallel to the sill at depths of 30–50 km, with two thrust events, also parallel to the sill, that are deeper and further to the NE. Near the eastern side of the Caspian are five thrusting earthquakes at 30–40 km, all of which have nodal planes dipping gently N to NE, and two strike-slip events.

Following Priestley *et al.* (1994), we doubt that the offshore earthquakes on the sill represent the motion between Eurasia and the southern Caspian: they are too deep and the normal faulting is inconsistent with the folding and shortening seen at the surface in industry seismic reflection data. There are insufficient earthquakes with reliable depths to define a dipping seismic zone offshore and a cross-section of earthquake depths is uninformative. Nonetheless, because of the clear pattern of focal mechanisms, we suspect that these earthquakes are related to the NE subduction of the south Caspian basement beneath the Apsheron–Balkhan sill. We expect that the normal faulting on or south of the sill is related to bending of the South Caspian lithosphere, analogous to that on the outer rises of oceanic trenches, or possibly to the detachment of a sinking slab that has broken away from the Earth's surface. The deeper thrust faulting NE of the sill, with steeply NE-dipping T axes, would then represent down-dip elongation of the subducting slab, which is again common at shallow depths in the oceans (e.g. Isacks & Molnar 1969). There is no evidence that the seismicity extends deeper than ~100 km, suggesting that subduction has not yet progressed far, either because it is slow or young. The shortening at the surface appears to be mostly aseismic offshore, with the sediments presumably decoupled from their underlying basement by the overpressured mud. The five thrust-faulting earthquakes on the eastern shore may represent an eastern seismic continuation of the northward underthrusting postulated offshore. We discuss the role of this suggested subduction in the regional tectonics later.

3.3 The Kopeh Dag

The Kopeh Dag forms a NW–SE range of mountains separating the Turkmen (Turan) shield from central Iran. The belt is up to 3000 m in elevation, rising 2000 m above the Turkmen plains. It is highest and narrowest in its centre and the east, becoming broader and lower towards the west, where it merges with the lowlands of the SE Caspian shore. The range is asymmetric, with a steep, linear and narrow NE side on which short, straight streams run directly from the high ground to the Turkmen plain. Its SW flank contains gentler slopes, is less regular, and contains a broader, more developed drainage network. The NE flank of the Kopeh Dag is assumed to be underlain by 'Hercynian' basement of the Turan shield, while the range itself contains thick Jurassic–Cretaceous marine sediments overlain by Eocene marls with some andesitic volcaniclastic horizons. These in turn are overlain by thick marine Pliocene units in the west (which continue into the South Caspian Basin) merging eastward into a continental sequence of equivalent age, reflecting the diachronous emergence of the range. Although there is some evidence for local structural detachments in Jurassic evaporites, most of the late Cenozoic and active folds in the Kopeh Dag are thought to have developed in the hanging-walls of basement-cored thrusts (Lyberis & Manby 1999). There is no evidence for major salt thicknesses that can produce large-scale regional decollement levels, as in the Zagros (Falcon 1969, 1974).

Earthquakes in the Kopeh Dag involve mostly right-lateral strike-slip faulting trending N to NNW or reverse faulting parallel to the NW regional strike (Tchalenko 1975; Berberian 1981; Jackson & McKenzie 1984). The abrupt linear topographic front forming the NE margin of the Kopeh Dag follows a fault zone referred to as the Main Kopeh Dag or Ashkabad Fault. This fault zone was associated with a large (M_s 7.2) earthquake in 1948, the focal mechanism of which remains uncertain (e.g. Rustanovich & Shirakova 1964; Jackson & McKenzie 1984) and where the co-seismic surface ruptures were ambiguous (Tchalenko 1975; Berberian & Yeats 2001). Nonetheless, it is

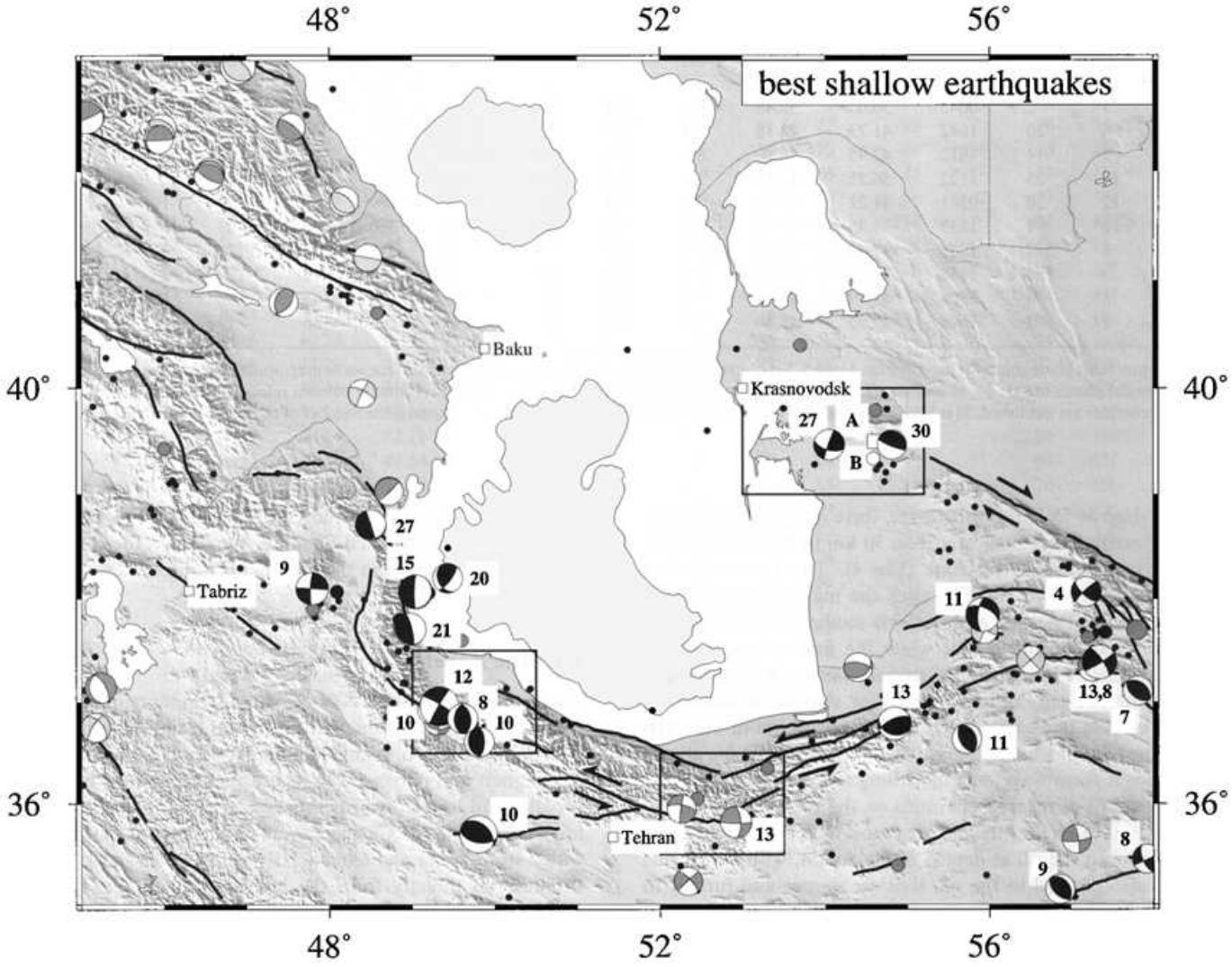

Figure 4. A compilation of the best-quality shallow earthquake focal mechanisms around the South Caspian Basin. Black focal spheres are for earthquakes where the mechanisms and centroid depths (all $\leq$30 km, shown in bold type) are constrained by body wave modelling (Table 1). Grey spheres are Harvard CMT solutions for events with $M_w \geq 5.3$ and with $\geq$70 per cent double-couple component the CMT depths of which were $<$30 km (see Table 2). Light grey focal spheres are first-motion fault plane solutions where the polarities were read on long-period instruments of the WWSSN (Table 3). Small black-filled circles are hypocentres of 1964–1998 events with $<$30 km depth from the catalogue of Engdahl *et al.* (1998). Large grey and black-filled circles are epicentres of other earthquakes of $> M_s$ 6.0 ($> M_s$ 7.0 for larger size) from 1900 to 1962 and post-1963, respectively. The trends of the major known faults onshore are marked by solid lines, taken from Fig. 3. Boxed regions are shown in greater detail in Fig. 7. In the box on the eastern Caspian shore, the white square A and the white circle B are the epicentres of the 1895 Krasnovodsk and the 1983 Kum Dag earthquakes, respectively. The grey region offshore is bathymetry deeper than 500 m.

clear from re-triangulation after 1948 (see Berberian & Yeats 2001 for a discussion), from offset man-made structures such as walls and irrigation systems (Trifonov 1978) and from geological evidence (Lyberis & Manby 1999) that the overall character of this fault zone involves right-lateral and reverse movement. Other earthquake mechanisms, such as that of 2000.08.22 (depth 4 km, Fig. 4) and 2000.09.19 (in Fig. 6, because of the CMT depth of 35 km) confirm the range-parallel right-lateral faulting near the NE topographic front (see Fig. 8 for slip vectors). Further SW, within the interior of the Kopeh Dag, both field observations (Tchalenko 1975) and earthquake mechanisms (Figs 4 and 5) show that the strike-slip faulting is more oblique to the trend of the range, with slip vectors of 330–350°, rather than 310–320° further NE (Fig. 8). Our observations support the conclusion of Lyberis & Manby (1999) that the convergence across the range as a whole is oblique right-lateral in character. We expect that the strike-slip faulting within the range, which strikes NNW at an oblique angle to the belt, rotates anticlockwise about a vertical axis as the deformation progresses to eventually become parallel to the regional strike (e.g. Jackson & McKenzie 1984; Jackson *et al.* 1995).

Lyberis & Manby (1999) point out that the structures of the Kopeh Dag continue NW to the Cheleken peninsular and Balkhan regions, becoming increasingly buried by sediment. This continuation is also seen in the earthquake mechanisms (Figs 4, 6 and 7c), which show both thrusting with NE slip vectors and NW–SE right-lateral strike-slip (Fig. 8). Two earthquakes in the region of Fig. 7(c) were associated with co-seismic surface faulting (Trifonov *et al.* 1986). The Kum Dag earthquake,

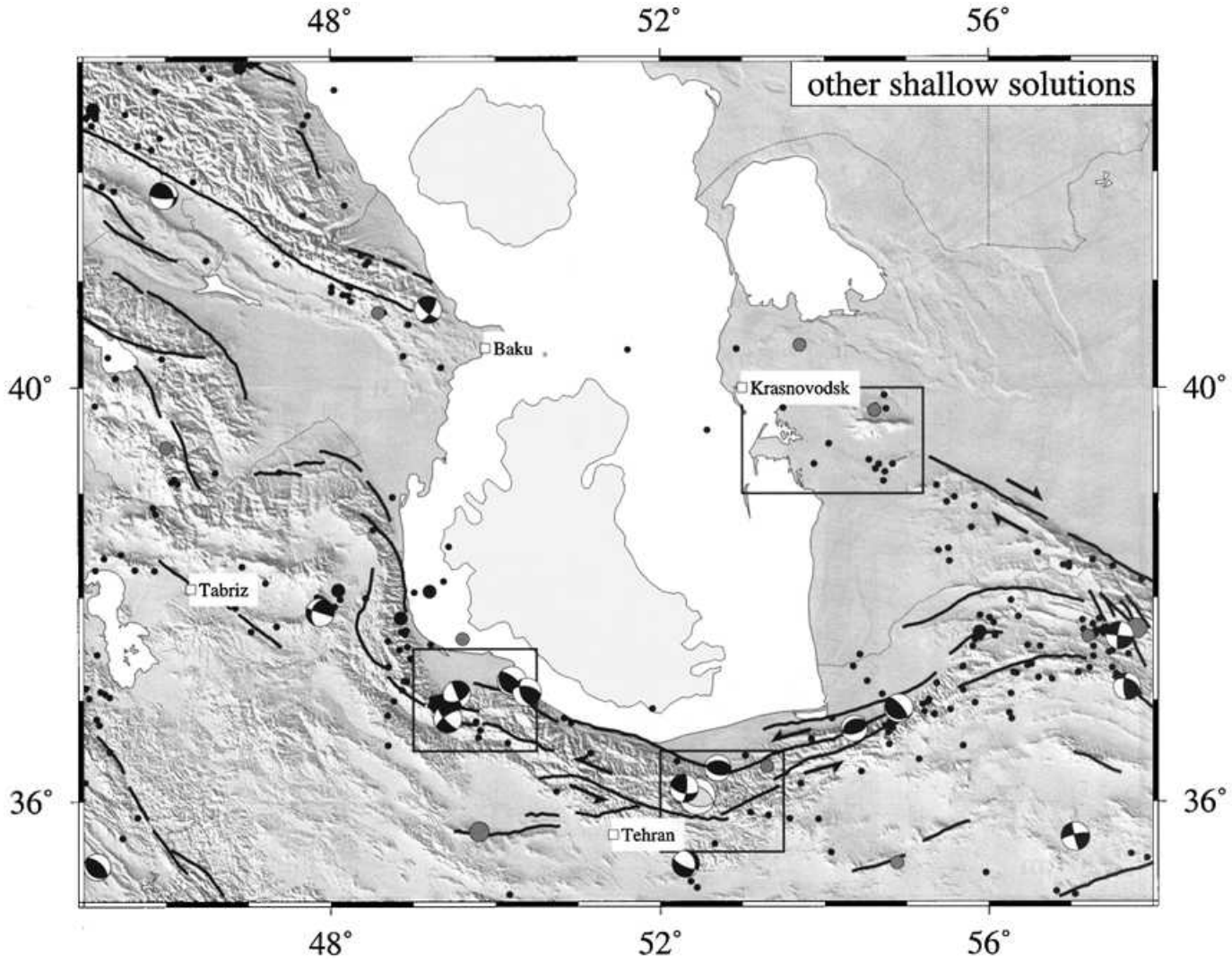

Figure 5. A compilation of all other CMT solutions not in Fig. 4 (black spheres) with reported depth <34 km from the Harvard catalogue from 1977 through 2001 January (Table 2), regardless of size and double-couple component. A single light- grey sphere NE of Tehran is a first-motion solution for the 1957.07.02 earthquake (Table 3), from McKenzie (1972). Other epicentres, faults, bathymetry and insets are as in Fig. 4.

on 1983.03.14 (m_b 5.2) produced WNW-trending right-lateral faulting with up to 40 cm offset, but was too small for us to analyse its waveforms. The Burun earthquake, on 1984.02.22 (M_w 5.7), produced en-echelon right-lateral cracks over a distance of $\sim$10 km with offsets up to $\sim$8 cm and a trend of 280°. The waveforms of this second earthquake were analysed by Priestley *et al.* (1994), who confirmed this mechanism and estimated the centroid depth at 27 km. The co-seismic ruptures of the Burun earthquake coincide with a well-known right-lateral strike-slip fault zone, where the associated structures form the Burun oil field. The curiosity about the Cheleken–Balkhan area is that the earthquakes are significantly deeper (27–31 km) than those in the Kopeh Dag (all <15 km), presumably because the active structures are buried deep beneath the sediments of the old Oxus river delta (which once entered the Caspian Sea in this region before being diverted north to the Aral Sea). The epicentre of the Krasnovodsk earthquake of 1895.08.05 (M_s 7.4) was probably in this region, though its focal mechanism and depth are unknown (Ambraseys 1997).

Thus the overall deformation of the entire belt from the Cheleken to the Kopeh Dag is characterized by oblique right-lateral shortening. There are indications in the earthquake mechanisms and their slip vectors (Fig. 8) that this motion is, to some extent, achieved by separating ('partitioning') the shortening and strike-slip components on to separate faults. Lyberis & Manby (1999) reach the same conclusion from geological evidence, and estimate that 75 km of overall N–S shortening in the western Kopeh Dag–Balkhan region over the last 5 Myr has been resolved into 70 km of shortening and 35 km of right-lateral offset on the Ashkabad fault. Such partitioning is common in the circum-Caspian region and we discuss it more later.

East of 56°E the shortening in the Kopeh Dag represents motion between the Turkmen shield and Iran. NE of the Ashkabad fault a large free-air gravity low shows a clear flexural signal, indicating that the shield is thrust SW beneath the mountains, with an effective elastic thickness of $\sim$12 km (Maggi *et al.* 2000a). The flexural signal in the gravity is lost west of 56°E, where the subdued topography and fewer earthquakes are likely to represent smaller motion between the Turkmen shield and the SE Caspian lowlands, rather than between the shield and Iran itself. This difference is seen in the

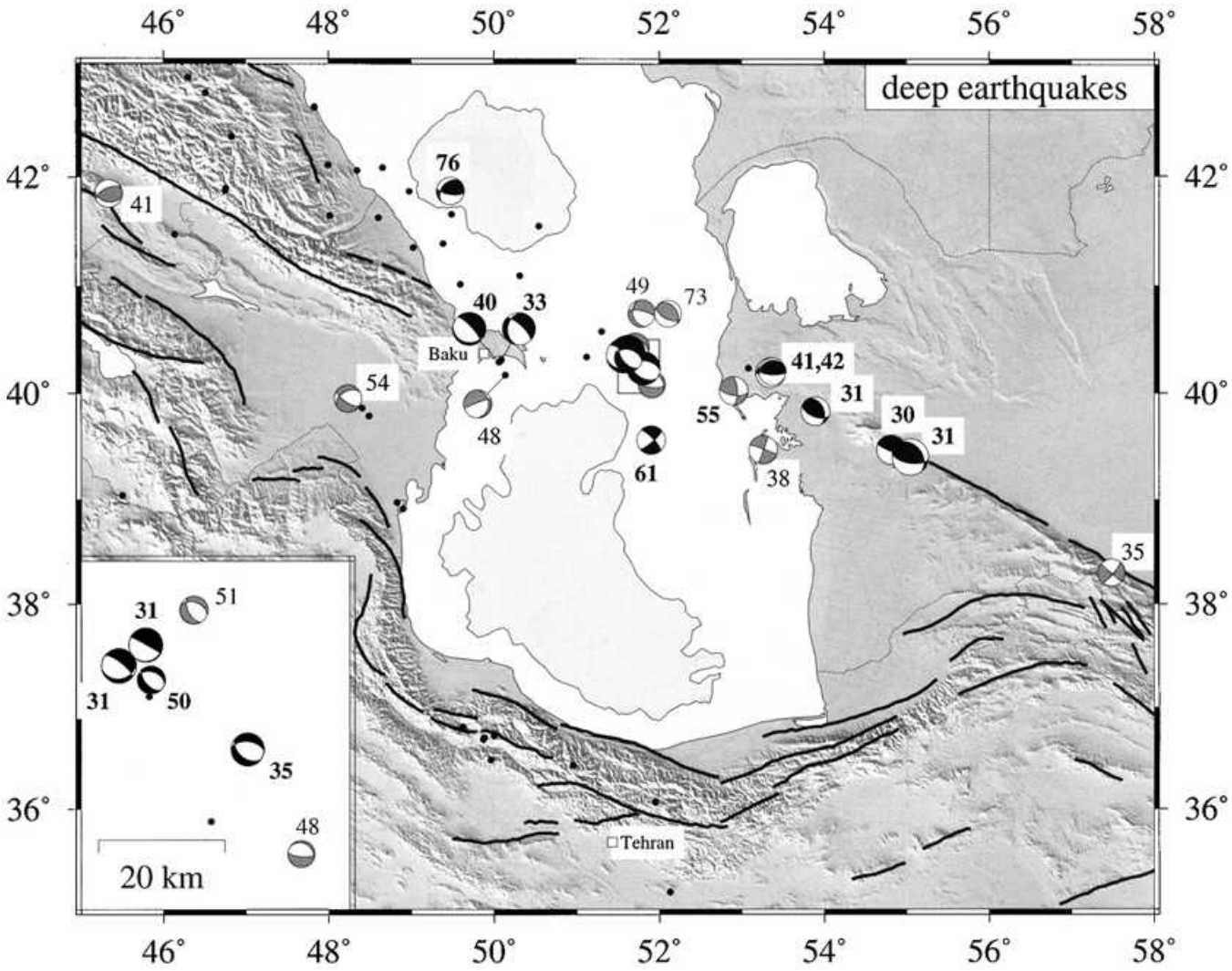

Figure 6. The deeper earthquakes in the South Caspian Basin region. Black spheres are events where the depths (in km, in bold) are constrained by waveform modelling to be ≥30 km (Table 1). Grey spheres are all Harvard CMT solutions, regardless of size and double-couple component, with reported depths of >33 km, but numbers next to these spheres are their depths from the catalogue of Engdahl *et al.* (1998). Small filled black circles are 1964–1998 hypocentres from the Engdahl *et al.* (1998) catalogue with reported depths of >60 km. Bathymetry and faults are as in Fig. 4. The outlined box in the central Caspian on the main map is enlarged as an inset in the lower left-hand corner.

polarity of the thrust faulting: west of 56°E the north overthrusts the south on gently N- or NE-dipping planes (Fig. 6), whereas on the Kopeh Dag range front east of 56°E it is clear from the topography, gravity and geology that the south overthrusts the north.

3.4 The Alborz

The Alborz forms a high arc of mountains from the southern end of the Talesh (~37°N 49°E) to their junction with the Kopeh Dag at about 56°E. The range is higher than the Kopeh Dag, with many summits in the range 3600–4800 m, culminating in the Quaternary volcano of Damavand (5671 m) in the centre of the belt (Fig. 7b). With its restricted width of 60–120 km, the Alborz is extremely steep, with the flanks abruptly joining the plains along major thrust faults on both sides [the Mosha, North Tehran and North Qazvin faults on the south side and the Khazar fault on the north side: Fig. 7(b), Berberian & Yeats (1999)]. The range contains a thick sequence of Paleogene andesitic volcanics and intrusive rocks, and appears to have separated two independent marine sedimentary basins in the Neogene: the South Caspian Basin to the north and a Miocene (Qom Formation) basin in central Iran to the south (e.g. Stöcklin 1974; Berberian & King 1981). Dating of thermal histories of granites in the central Alborz suggests rapid uplift of the range between about 6 and 4 Ma, nearly synchronous with subsidence in the South Caspian (Axen *et al.* 2001). Today, the Sefid Rud is the only river to cross the Alborz from central Iran to the Caspian, which it does through the deep gorge at Rudbar and Manjil (Fig. 7a).

All the well-constrained earthquake depths in the Alborz are <15 km (Fig. 4) and though there are a few listed as >60 km in the EHB catalogue (Fig. 6) they are all small and we cannot confirm them. Most of the focal mechanisms in this belt show either reverse faulting or left-lateral strike-slip on faults parallel

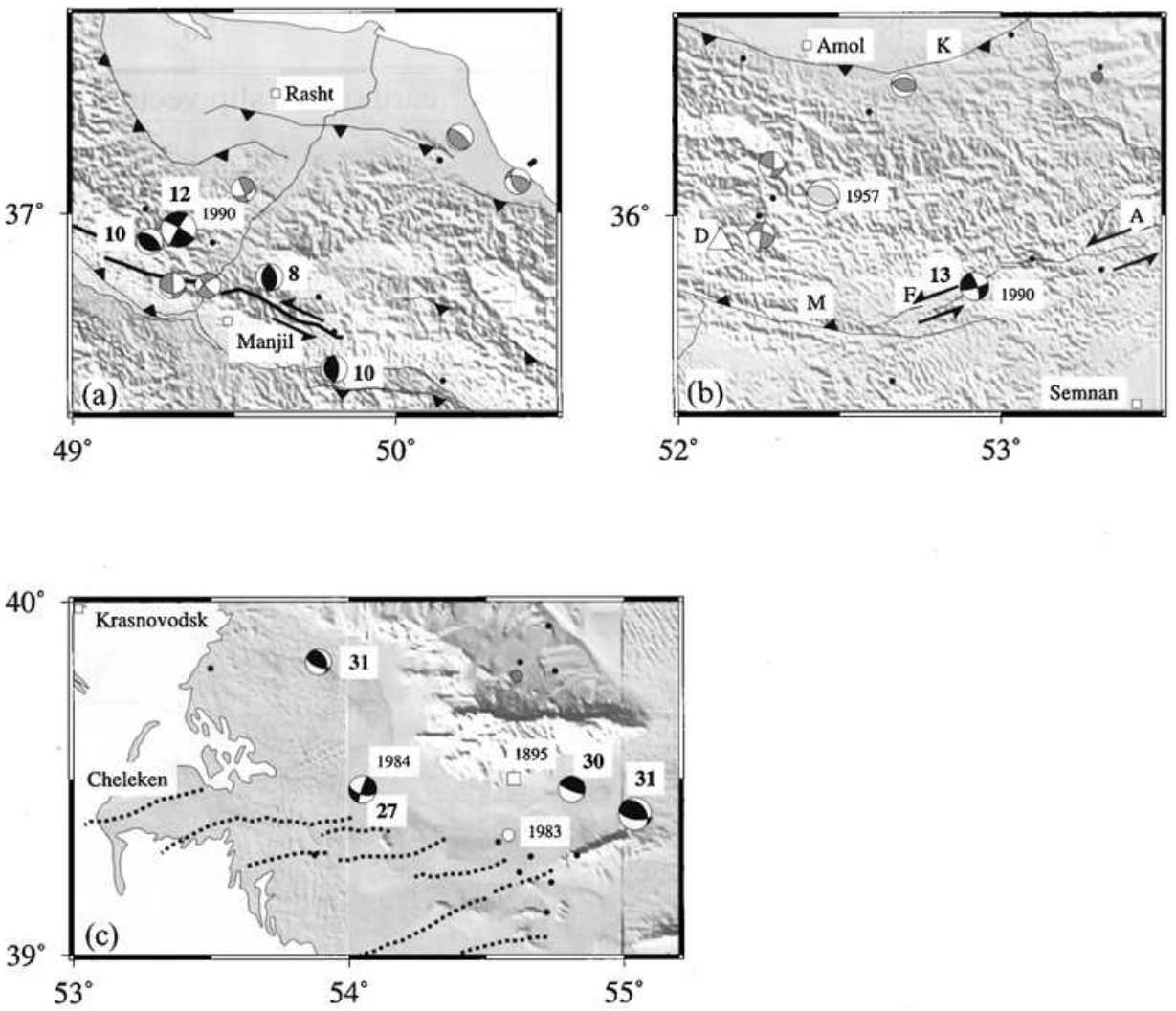

Figure 7. Enlarged boxed regions in Fig. 4, all of which show the slip partitioning on subparallel thrusts and strike-slip faults that is so common around the South Caspian Basin. Focal sphere shading is as in Fig. 4. (a) The western Alborz region of the 1990 Rudbar–Tarom earthquake (marked 1990), the left-lateral co-seismic surface ruptures of which (Figs 9a and b) are marked by thicker lines than the other faults (Berberian *et al.* 1992). (b) The region of the 1957.07.02 earthquake in the eastern Alborz. Marked faults are the Mosha (M), Firuzkuh (F) and Astaneh (A) faults, from Berberian *et al.* (1996). D is the Quaternary volcano Damavand. The 1990.01.20 earthquake at Firuzkuh (M_w 5.9) is marked 1990 and its focal mechanism and depth (13 km) are those suggested by the body wave analysis in the Appendix (Fig. A1). Figs 9(c) and (d) show aerial photos of the Firuzkuh and Astaneh faults. (c) The Cheleken–Balkhan region. The approximate epicenter of the 1895 Krasnovodsk earthquake is marked by the white square. That of the 1983.03.14 Kum Dag earthquake is marked with a white circle. The dashed lines are anticline axes of major folds affecting the Pliocene Red Series and younger sediments. Note the right-stepping pattern typical of right-lateral strike-slip motion at depth.

to the regional strike of the belt (Figs 4 and 5). Many young reverse faults and folds are known in the Alborz, though none are known to have ruptured at the surface in modern earthquakes (e.g. Berberian 1976; Berberian & Yeats 1999).

Evidence for left-lateral strike-slip parallel to the belt is now substantial. Up to 80 km of left-lateral co-seismic surface ruptures formed in the 1990.06.20 (M_w 7.3) Rudbar–Tarom earthquake (Figs 9a and b; Berberian *et al.* 1992). The 1970.07.30 Karnaveh earthquake (M_w 6.4) is also thought to have involved left-lateral faulting, based on the alignment of its aftershock zone (Jackson & Fitch 1979). Other left-lateral faults are known in the field and from air photographs (e.g. Wellman 1966; Berberian *et al.* 1985, 1996; Hessami *et al.* 1997; Berberian & Yeats 1999). An interesting feature of the range-parallel left-lateral strike-slip faulting is that it is much clearer in the eastern Alborz than in the west. A number of such faults are clear on the ground and on air photographs (Figs 9c and d) east of about 52°E (Berberian *et al.* 1985, 1996). In contrast, the 80 km of coseismic left-lateral ruptures that were observed following the 1990 Rudbar–Tarom earthquake in the western Alborz (Berberian *et al.* 1992) occurred on a fault system that was previously unknown and has a much more subtle expression in the geomorphology. The Rudbar–Tarom strike-slip fault is located in very high ground, mostly above 2000 m and close to the crest of the western Alborz. Only in a few places is it recognizable on air photographs or satellite images. Our conclusion, reinforced by a further field study in 2000 by Berberian and Jackson, is that the Rudbar–Tarom earthquake fault probably does not move often enough to exert much influence on the geomorphology (in contrast to the left-lateral faults

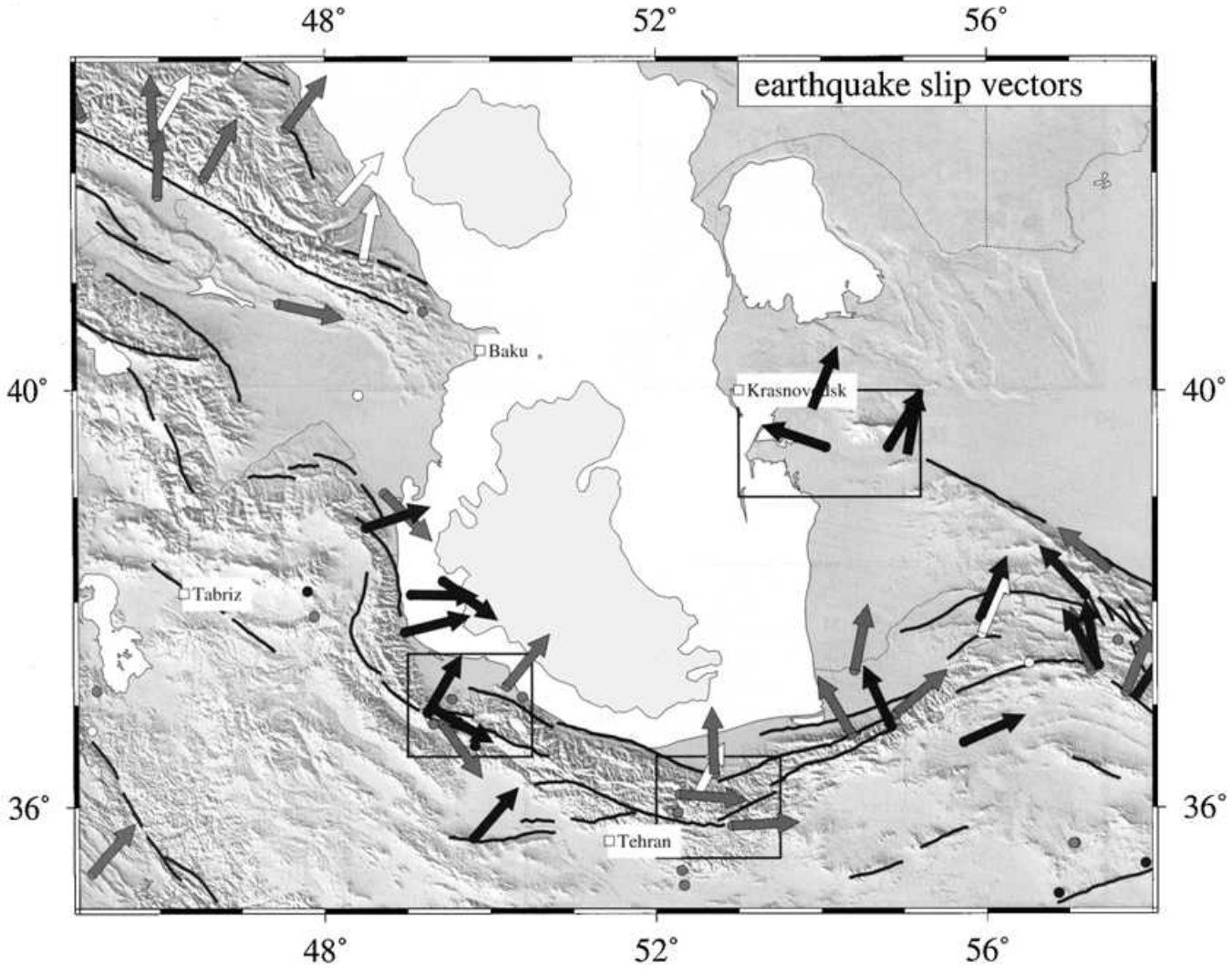

Figure 8. Horizontal projections of slip vectors of shallow earthquakes round the South Caspian Basin. Because of the two possible fault planes in each fault plane solution, only events for which slip vectors are listed in Tables 1 and 2 have been plotted. This includes: (a) strike-slip events the fault planes of which are known from surface ruptures or from nearby faults; (b) thrusting events the fault planes of which can be identified from the nearby topography, or where the rake is so close to 90° that the identification of the fault plane is unimportant. To avoid more than one slip vector per earthquake, they were chosen in hierarchy: (1) black arrows for events where the mechanisms are constrained by body wave modelling; (2) grey arrows are for Harvard CMT events; (3) white arrows are for first-motion solutions. Arrows are plotted to show the motion of the south or west side relative to the north or east. Epicentres of other earthquakes in Figs 4 and 5 are marked by circles (black for solution constrained by waveform modelling, grey for CMT solutions, white for first-motion solutions).

further east), and that the fault would almost certainly have remained unrecognized were it not for the 1990 earthquake. We suspect that this contrast between the expression of the left-lateral faults in the eastern and western Alborz is significant, and return to this issue later.

Finally, there are a few mechanisms showing thrust faulting on planes perpendicular to the regional strike (Figs 4, 5 and 7a). Two of these were aftershocks of the 1990 Rudbar–Tarom earthquake (Fig. 7a) and may be associated with the terminations of strike-slip fault segments, as has been seen elsewhere (Bayasgalan *et al.* 1999). There is also a Harvard CMT solution for a small earthquake (1988.08.23, M_w 5.1) SE of Tehran, apparently with a normal-faulting mechanism (Fig. 5). The waveforms for this event were too small for us to confirm its mechanism by our modelling techniques, and we cannot assess the reliability of this CMT solution, which is clearly unusual in the Alborz region.

The Alborz accommodates the overall motion between the southern Caspian and central Iran, and seems to involve oblique left-lateral shortening. Once again, the earthquake slip vectors indicate that this is achieved by a spatial separation, or 'partitioning', of the strike-slip and reverse components on to subparallel faults with orthogonal slip vectors (Fig. 8). There is abundant evidence for recent uplift in the Alborz, in the form of incised river terraces and coastal marine terraces, and it is very likely that the crust of Iran is being thrust over the South Caspian Basin (Berberian 1983). However, there is no convincing evidence in the earthquake focal depths for current subduction of the Caspian Sea crust into the mantle beneath the Alborz, as there is on the Apsheron–Balkhan sill. We discount the few small earthquakes at depths >60 km in the EHB catalogue shown in Fig. 6, most of which occur in the Rudbar–Tarom region where a local microearthquake survey found no activity deeper than ~20 km (D. Hatzfeld, private communication,

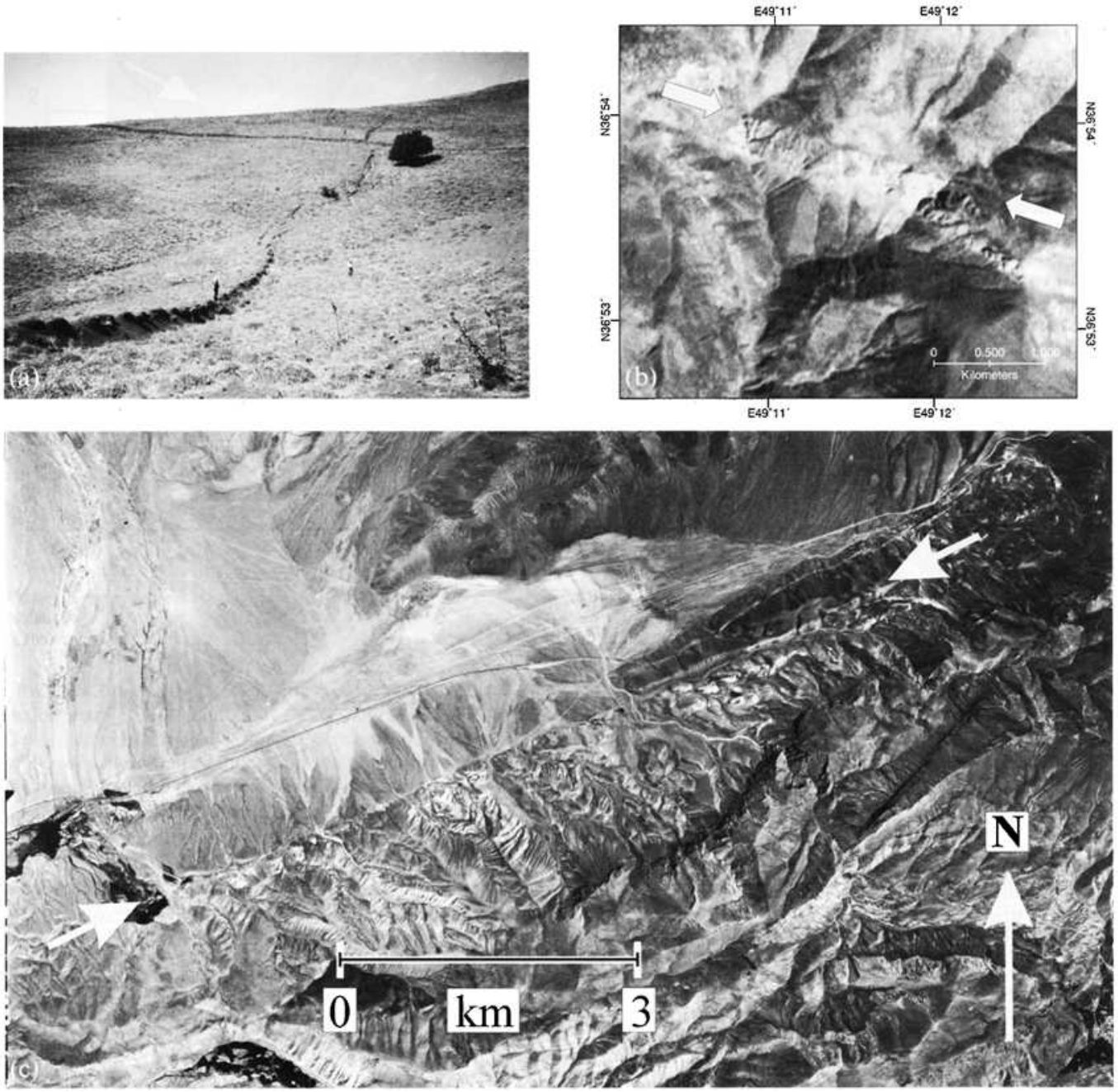

Figure 9. (a) The left-lateral surface rupture of the 1990 Rudbar–Tarom earthquake (M_w 7.3) near Jaishabad (36°54.0′N, 49°10.1′E) in the western Alborz, photographed in 2000 September, 10 years after the earthquake. This rupture connects the Kabateh and Baklor fault segments described by Berberian *et al.* (1992), which are now known to be continuous. The view is to the west, with the north side dropped by ~1 m, in the opposite sense to the local topography (see Fig. 9b). The left-lateral component was visible on the ground, but could not be measured accurately 10 years after the earthquake. (b) LANDSAT 7 TM image of the 1990 Rudbar–Tarom strike-slip fault at Jaishabad (Fig. 9a). The fault is visible between the white arrows, mostly because its vertical component (down to the north) is in the opposite sense to the local topography, and has caused streams crossing the fault from N to S to incise on the southern side. This is one of the very few locations where the 1990 ruptures are clearly associated with a feature that is clear in the geomorphology. (c) Aerial photo of the left-lateral Firuzkuh fault, near 53°E (see Fig. 7b and Berberian *et al.* 1996). The fault is visible between the white arrows. (d) Air photo of the left-lateral Astaneh fault near 53.5°E (Fig. 7b). The Astaneh fault runs between the big white arrows. Smaller arrows show beheaded streams flowing from NW to SE, now offset in a left-lateral sense.

2001). In this respect, the significance of the Quaternary stratovolcano of Damavand (Fig. 7b), northeast of Tehran, remains enigmatic. Berberian (1983) estimates about 25 per cent shortening (perhaps ~50 km) of the Alborz during the Pliocene and Pleistocene.

3.5 The Talesh

The Talesh forms a N–S range along the western coast of the Caspian in Iran and Azerbaijan. Geographically, the Talesh is a westward continuation of the Alborz, but is narrower (typically

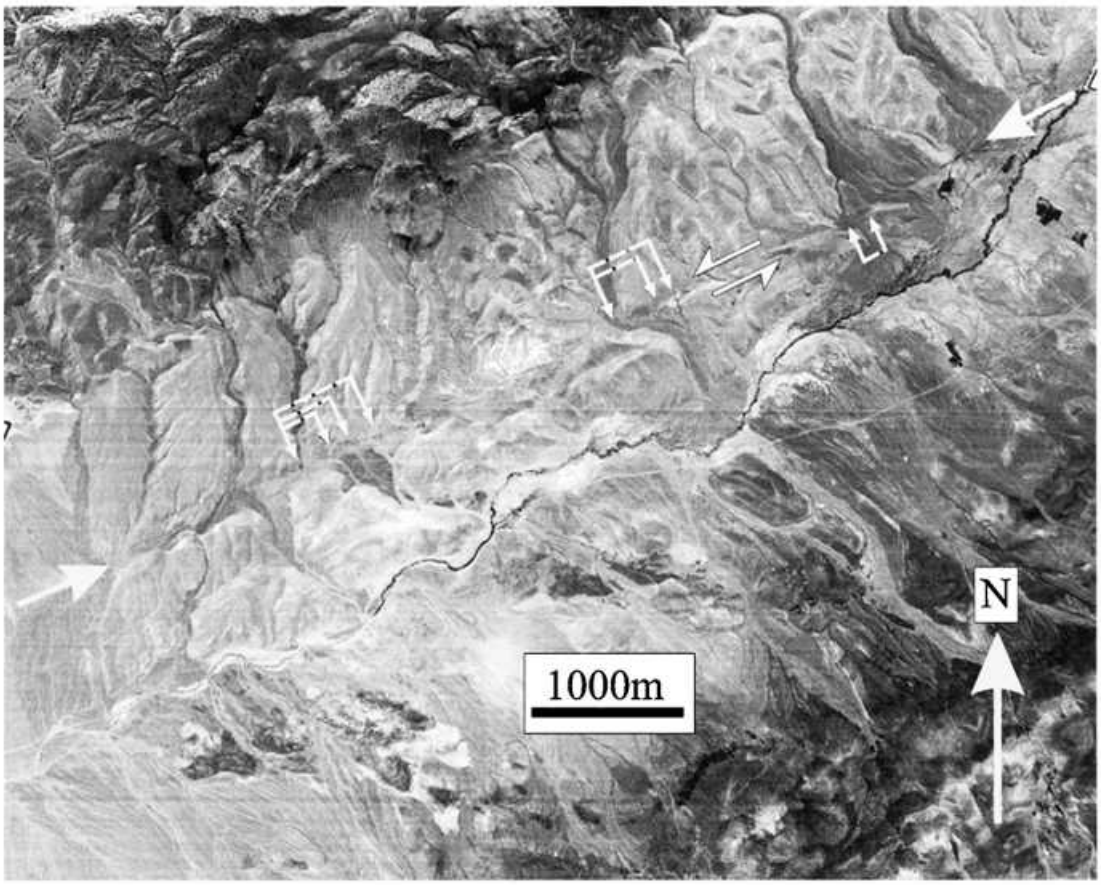

Figure 9. (*Continued.*)

only < 50 km width). It contains many of the same rocks as the Alborz, including the thick Paleogene andesitic volcaniclastic sequence. The steep and heavily forested eastern flank of the Talesh is scored by narrow ravines and defiles formed by short, torrential streams plunging towards the Caspian, but none cross the entire range. The structure is dominated by N–S folds and thrusts which swing smoothly into an E–W trend at the northern end of the range (39–40°N) where it meets the flat plains of the Kura Basin (Fig. 3; Berberian 1997).

The earthquake mechanisms in the Talesh are quite distinct from those in the Alborz: they indicate thrusting on almost flat faults (rare in the Alborz) at depths of 15–26 km (deeper than in the Alborz), with slip vectors directed towards the Caspian Sea (Figs 4, 5 and 8). The locations of these events are all close to the coastline and significantly west of the N–S fold axes offshore that are so important for the oil industry (Fig. 3). The centroid depths of these earthquakes place the active faults close to the base of the sedimentary section in the western Caspian (Fig. 2) so that they are likely to represent thrusting of the crystalline basement of the Caspian westwards beneath the Talesh mountains (Fig. 10). It is possible that these low-angle thrusts continue to the surface some distance offshore where the surface folds are observed, but more likely that the surface sediments are decoupled from the basement by the overpressured mud, and that the offshore folds simply reflect shortening of the sedimentary cover in response to deeper convergence further to the west. Sliding of the offshore cover above the decollement horizon is encouraged by the uplift of the mountains in the west and the steep topographic gradient from west to east.

There is no indication in either the location of the seismicity or in the focal mechanisms for substantial offshore faulting in the basement on the west side of the southern Caspian basin. There is consequently no support in this data set for the major N–S basement faults offshore that are such a common feature in the Russian literature (e.g. Shikalibeily & Gigoriants 1980). Nor is there any sign in the earthquake mechanisms of N–S right-lateral strike-slip faulting in the Talesh, though this is drawn on some maps (e.g. Karakhanian *et al.* 1997; Nadirov *et al.* 1997). Preliminary fieldwork by M. Allen and colleagues at the Geology Institute of Azerbaijan, summarized in Fig. 10, suggests about 25 km (or 30 per cent) shortening in the Talesh since the late Miocene, based on the assumption that exposed thrusts and folds link into a major thrust system beneath the range.

3.6 The eastern Greater Caucasus and Kura Basin

The Greater Caucasus forms a relatively narrow (100–200 km) but high range that decreases in elevation from 4000 to 5000 m near its centre to die out eastwards at the Caspian shoreline on the Apsheron peninsula. Metamorphic rocks are exposed in the core of the range and are the poorly understood products of Paleozoic and/or Triassic orogens on the southern edge of the Russian platform. Early Jurassic extension led to the deposition

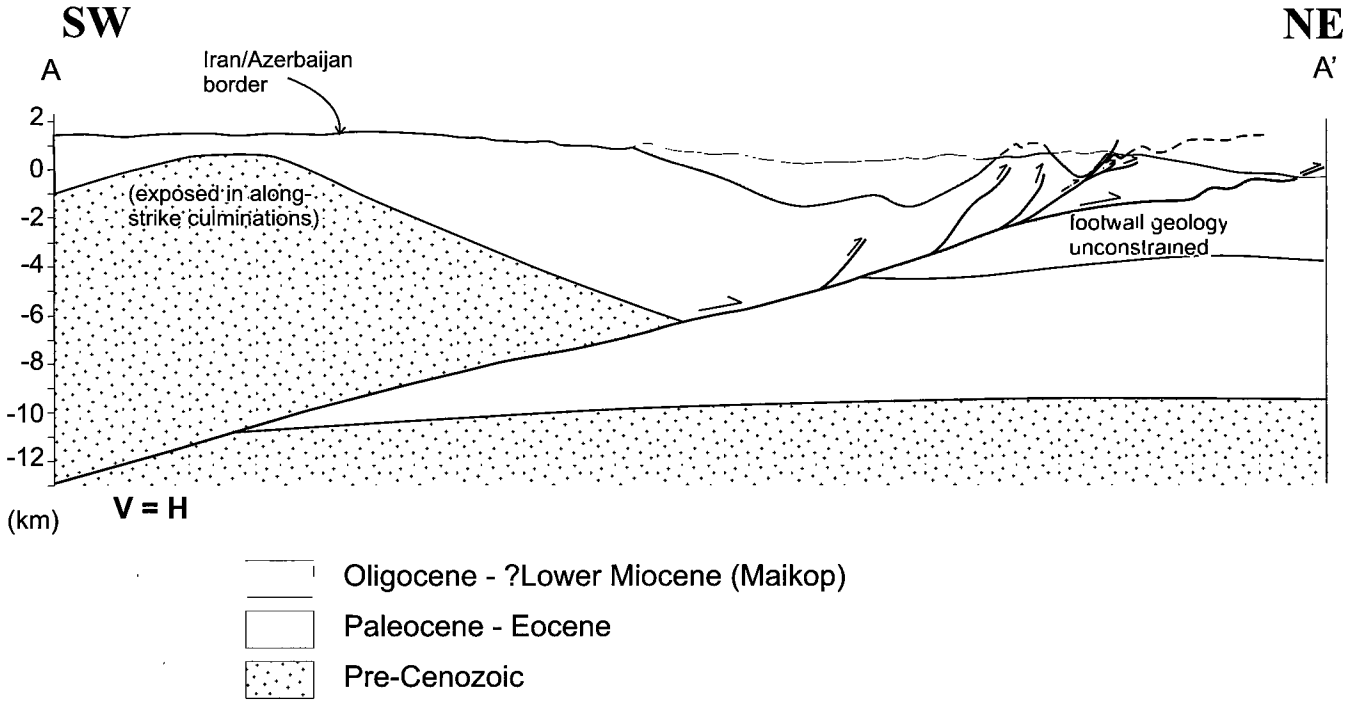

Figure 10. A schematic geological cross-section of the NE Talesh in Azerbaijan (see Fig. 3 for location), drawn to reconcile the earthquake and surface data. Most large earthquakes are on the basement thrusts at 10–20 km depth beneath the Iran–Azerbaijan border, whereas the surface folding in the young sediments occurs further NE and offshore, where the thrusts reach shallower levels. The vertical and horizontal scales are equal.

of a thick, deep marine clastic succession, followed by continued marine deposition through the Cretaceous and early Cenozoic, with marginal carbonate platforms flanking a zone of deeper water. Major exhumation and uplift of the range did not begin until the late Cenozoic, possibly as recently as the late Miocene, presumably consequently, of the Arabia–Eurasia collision (e.g. Philip *et al.* 1989).

Most of the available earthquake mechanisms in the eastern Greater Caucasus show low-angle thrusting on planes dipping gently towards the mountains on both sides (Figs 4 and 5). In Dagestan, on the northern side, young thrust faults that cause uplift and incision of drainage and which follow the trend of the Caspian shoreline between 43 and 41°N are particularly clear on satellite images (see Jackson & McKenzie 1984). It is in this region that the range bulges north and where a series of destructive earthquakes involving such thrusting occurred in 1970 May (Fig. 4; Table 3). Slip vectors in the eastern Greater Caucasus are generally directed NE (Fig. 8) in spite of the Arabia–Eurasia convergence being approximately N–S at this longitude. The reason for this anomaly is that overall convergence is 'partitioned' into its separate strike-slip and shortening components on a regional scale, with a NW–SE right-lateral strike-slip dominating in eastern Turkey and NW Iran, while NE–SW-directed shortening occurs in the eastern Greater Caucasus. This was first noticed in the earthquake focal mechanisms (Jackson 1992; Jackson & Ambraseys 1997) and has now been confirmed by GPS measurements (see Fig. 10, McClusky *et al.* 2000). The NE side of the eastern Caucasus, such as the Kopeh Dag, shows a large free-air gravity low, with the characteristic shape of a flexural foreland basin and an effective elastic thickness of 16 km (Maggi *et al.* 2000a). This indicates that the eastern Greater Caucasus is being thrust over the southern edge of the Russian platform, but there is no indication in the seismicity of subduction of material into the mantle.

On its south side, the eastern Caucasus is also being thrust over the sediments of the Kura depression (Fig. 3), with substantial ($M_s \leq 7$) earthquakes in 1668 and 1902, probably associated with the major north-dipping thrusts (Berberian 1997). Some earthquakes occur beneath the Kura Basin, but their significance is enigmatic. There is one poor first-motion solution in Fig. 4 from Jackson & McKenzie (1984) and a CMT solution showing oblique normal faulting, apparently at 54 km depth (Fig. 6). Jackson & McKenzie (1984), impressed by the straightness of the Araxes river, suggested that a NE-SW strike-slip fault followed the Iran–Azerbaijan border between 46°E and 48°E, but we are unaware of any real supporting evidence for such a fault.

4 DISCUSSION

4.1 Motion of the South Caspian Basin relative to its surroundings

The almost complete lack of shallow earthquakes within the South Caspian Basin itself indicates that it behaves as a rigid block within the Eurasia–Iran–Arabia collision zone. We reach this conclusion in spite of abundant folding of the sedimentary cover offshore, which we do not believe indicates faulting of its underlying basement. Instead, the surface folding is likely to be completely decoupled, and can be spatially separated, from any basement shortening by the overpressured muds. Thus the N–S folds in offshore Azerbaijan are probably a response to deeper basement shortening that occurs ~100 km further west beneath the Talesh (Fig. 10), and the WNW–ESE surface folds near the Apsheron–Balkhan sill are probably a response to deeper thrusting of the southern Caspian beneath the northern Caspian. The lack of shallow earthquakes on the Apsheron–Balkhan sill indicates that this shortening is largely aseismic, which is

known in other places, such as the Hellenic Trench (Jackson & McKenzie 1988), where thick sediments choke the subduction zone. Fig. 3 shows other folds offshore from the SE Caspian lowlands in Turkmenistan. This area is totally aseismic and these folds are unlikely to be connected to any basement faulting: instead we expect them to be a response to sliding of the thick sandstones (the 'Red Series') above the overpressured mud, driven by the topographic slope from east to west. Other folds in the centre of the South Caspian Basin could also be a response to any of these factors, aided by mud diapirism.

If the South Caspian Basin is rigid, the deformation in the belts that surround it result from its motion relative to Iran and Eurasia. This is most clearly established in its eastern part, where a right-lateral component in the western Kopeh Dag (53–56°E) and a left-lateral component in the eastern Alborz (west of 56°E) indicate that the motion of the SE Caspian lowlands must have a westward component relative to Eurasia and Iran (Fig. 11a), in a geometry that resembles the expulsion of central Anatolia from the collision zone in eastern Turkey (e.g. McKenzie 1972). This westward component of motion enhances the underthrusting of the south Caspian basement beneath the Talesh.

Although left-lateral strike-slip is seen along the whole curved arc of the Alborz from 49°E to 56°E, we cannot use the shape of the arc to establish a pole of rotation for the South Caspian Basin because the overall motion is not pure strike-slip (unlike that of the North Anatolian fault in Turkey). Both the earthquake mechanisms and the geology indicate that considerable shortening accompanies the strike-slip in both the Alborz and western Kopeh Dag and, because we do not know the relative importance of these two components, we cannot determine the overall slip vectors or how they change along the strike of the belts. Nonetheless, some crude estimates of probable rates are possible. The overall Arabia–Eurasia convergence is known from a combination of Africa–Eurasia and Arabia–Africa motions to be approximately N–S at about 30–33 mm yr^{-1} at the longitude of the Caspian (Jackson 1992; DeMets *et al.* 1994; Jestin *et al.* 1994; Chu & Gordon 1998). Jackson & McKenzie (1984, 1988) and Jackson *et al.* (1995) suggest that about 10–15 mm yr^{-1} of this motion is accommodated in the Zagros mountains: an estimate that is very dependent on the assumptions they made, but which is roughly compatible with the ~50 km of shortening thought to have occurred in the Simple Folded Belt of the Zagros over the last 5 Myr (Falcon 1969, 1974). If ~15–20 mm yr^{-1} remains to be taken up across the Alborz and Apsheron–Balkhan sill, we can construct a velocity triangle, in the manner of Fig. 11(b). First, we observe that the left-lateral motion in the Alborz appears to die out in the west at about 49°E, where the regional trend and the strike of the left-lateral Rudbar–Tarom earthquake fault is about 300°. This suggests that the motion of the South Caspian relative to Iran is in the direction ~210°, or that angle the EIC in Fig. 11(b) is ~30°. If the angle EIC > 30° we would expect the left-lateral motion to continue further west as the arc of the Alborz swings into the Talesh; if EIC < 30° the left-lateral motion would not extend as far west as it does. These considerations are compatible with the strike-slip faulting being clearer and in lower topography east of 53°E, where the strike-slip component should be greater than in the western Alborz, where the strike-slip faulting is less obvious in the morphology is associated with higher mountains, and where thrust faulting should predominate. Secondly, the motion of the South Caspian

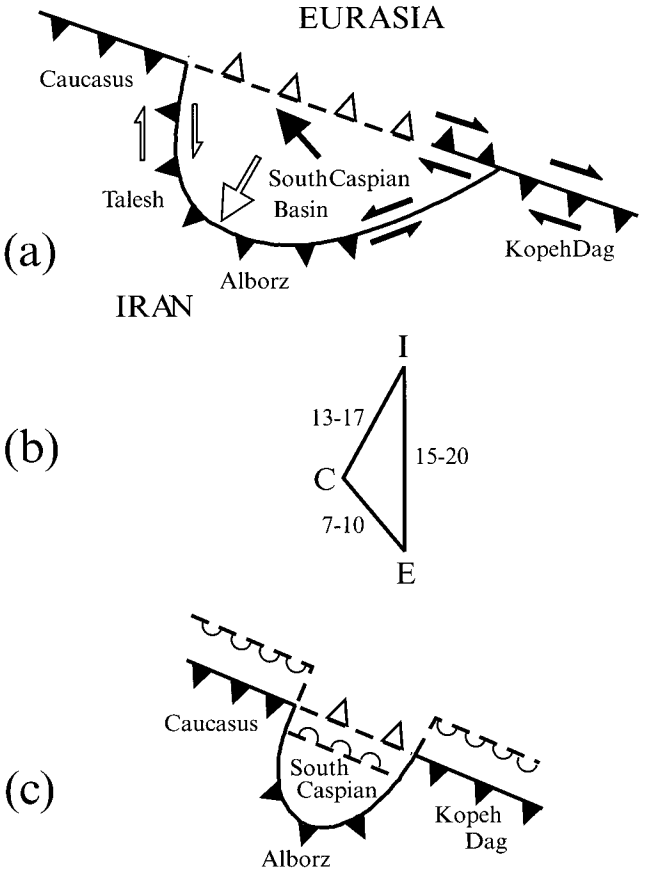

Figure 11. Sketches to illustrate the probable active tectonics of the South Caspian Basin. (a) The present-day configuration, showing S to SW underthrusting in the Kopeh Dag, Alborz, Talesh and eastern Greater Caucasus and north-dipping underthrusting in the central Caspian. Note the left-lateral strike-slip component in the eastern Alborz, and right-lateral component in the Kopeh Dag. The white arrow shows the approximate direction of the South Caspian Basin relative to Iran, and the black arrow shows its motion relative to Eurasia. (b) A velocity triangle constructed to illustrate the relative motion between Iran (I), Eurasia (E) and the South Caspian Basin (C). Velocities are in mm yr^{-1}. (c) A sketch to illustrate how the current collinear geometry of the seismic belt across the Apsheron–Balkhan sill with the Caucasus and Kopeh Dag is unstable because the underthrusting is to the north in the middle (white triangles) but to the south on either side (black triangles). It will eventually evolve to the offset configuration shown by the white semi-circles.

relative to Eurasia must have a shortening component and thus an azimuth that exceeds the 300° trend of the Kopeh Dag west of 56°W; or, in other words, the angle IEC in Fig. 11(b) must be less than 60°. These simple considerations suggest that the Caspian–Eurasia motion is at least 7–10 mm yr^{-1} in a direction somewhat north of 300°, and that the Caspian–Iran motion is no more than 13–17 mm yr^{-1} in the direction ~210°. However, we emphasize that these rates are very uncertain.

We can now compare these postulated rates and motions with the geological evidence. Shortening in the central Kopeh Dag since the Miocene is evidently compatible with ~15 mm yr^{-1} convergence between Iran and Eurasia (Lyberis & Manby 1999). We suspect that the earthquakes at 80–100 km beneath the Apsheron–Balkhan sill imply some subduction of the 'oceanic' South Caspian basement into the mantle, but it is not clear how much shortening this represents between the South Caspian

Basin and Eurasia, as we do not know the age or duration of the motion responsible. However, two observations suggest that the South Caspian–Eurasia shortening is both recent and relatively small in magnitude. First, there is no sign of recent volcanism north of the Apsheron–Balkhan sill, which might be expected if the deep earthquakes represent the declining activity in a subduction zone that has been active for some time. Secondly, the Greater Caucasus, Apsheron–Balkhan sill and the Kopeh Dag are all roughly collinear, yet the polarity of the underthrusting on the sill is opposite to that on either side: both the Greater Caucasus and the Kopeh Dag are overriding shields to the north, whereas the earthquakes and the bathymetry indicate that the central Caspian overrides the South Caspian Basin to the south. This configuration would soon evolve into a non-collinear geometry if it persisted for long (Fig. 11c).

Much of the deformation within the South Caspian Basin sediments is younger than about 3.4 Myr, with sediments older than this showing no thickness variations over the folds, while younger sediments thin on to the fold crests (Devlin *et al.* 1999). It is possible that some re-arrangement in the motions happened at this time, with shortening switching from the Alborz to the Apsheron–Balkhan sill. Prior to the Pliocene we know the Alborz was elevated from the coarse Neogene clastic sediments on both of its margins. If at that time most of the Iran–Eurasia convergence was concentrated in the Alborz, the South Caspian Basin would have been a deep, heavily sediment-loaded, elongated tongue of material protruding into Iran ~300 km in front of the Greater Caucasus and Kopeh Dag (Fig. 11c). It would perhaps be no surprise if it later broke along the narrow gap following the Apsheron–Balkhan sill, and if the lower South Caspian Basin then started to underthrust the higher and thicker crust on the northern side. Thus the entire present-day geometry of the deformation in the Southern Caspian Basin and its surroundings may date from about 3.4 Ma. The trigger for this postulated reorganization could be the initiation of shortening in the Simple Folded Belt of the Zagros (Falcon 1969, 1974), which perhaps heralded the final accretion into the collision zone of the various tectonic blocks within Iran, and the start of truly intracontinental shortening.

On the basis of Fig. 11(b) and the much higher topography in the Alborz than in the Kopeh Dag–Cheleken belt west of 56°E, we expect both the current shortening rates and the total amount of late Cenozoic shortening to be higher in the Alborz than on the Apsheron–Balkhan sill. If it is true that shortening has been concentrated in the Caucasus–Talesh–Alborz–Kopeh Dag arc, then we would also expect evidence for a N–S right-lateral shear between the Caspian and NW Iran in the Talesh, of which there is no sign in the earthquake mechanisms. N–S right-lateral strike-slip faults linking the eastern Caucasus with the Talesh are shown on various maps of Russian origin (e.g. Karakhanian *et al.* 1997; Nadirov *et al.* 1997), but it is not clear on what evidence their existence is postulated. Both Trifonov (1978) and Kopp (1997) show right-stepping en echelon folds and right-lateral strike-slip faults splaying NW–SE away from the thrusts west of Baku and entering the northern side of the Kura Basin. We are unaware of any convincing evidence that such faulting crosses the Kura Basin or enters the Talesh as N–S right-lateral strike-slip, though H. Philip (private communication, 2001) interprets an apparent right-lateral offset of the Kura river as evidence that such a N–S fault zone is active. At shallow levels, the strong curvature of the Talesh fold axes, from E–W in the north to N–S along the coast, could be related to a shear that has rotated the originally E–W folds clockwise to become parallel to the coast as the western (Iranian) side moves north past the Caspian. In this case, it may be that shear is distributed in the wedge of relatively weak sediment above the low-angle thrusts at 15–25 km rather than concentrated on to a strike-slip fault, while the E–W shortening component (related to the westward component of the Caspian's motion) is taken up by N–S thrusts. This is again a form of 'slip-partitioning', but without requiring a discrete strike-slip fault at the surface. It does not, however, explain the lack of any seismological evidence for N–S right-lateral shear at deeper levels. The E–W folds and thrusts in the northern Talesh are an important indication that on the west side of the Caspian some of the Iran–Eurasia shortening is taken up south of the Kura Basin, accounting for the relatively minor shortening in the eastern Greater Caucasus, represented by the decreasing elevation of that range as it approaches the Apsheron–Balkhan sill. The folds in the Kura Basin and offshore mimic this link between the Caucasus and Talesh, curving from E–W in the eastern Kura Basin to N–S offshore (Fig. 3). These folds are in regions of generally low seismicity, most likely because they are decoupled from their underlying basement by thick mud sequences.

In summary, it seems clear that the South Caspian Basin has a westward component of motion relative to both Eurasia and Iran, and that this enhances the underthrusting in the Talesh. The likelihood is that the basin moves SSW relative to Iran at ~10–15 mm yr^{-1} and NW relative to Eurasia at 8–10 mm yr^{-1}: but these are are not well-constrained estimates.

4.2 Slip partitioning round the South Caspian Basin

Part of the uncertainty in our estimates of the motion of the rigid South Caspian Basin arises from the ubiquitous 'partitioning', or separation of oblique convergence into its orthogonal strike-slip and reverse components on parallel faults, which is a feature of the Kopeh Dag, Alborz, and also the Caucasus-eastern Turkey region (Fig. 8). This is a common phenomenon in oceanic island arcs (e.g. Fitch 1972; McCaffrey 1992) and makes it very difficult to estimate overall convergence directions in such zones (e.g. DeMets *et al.* 1990). It is also common on the continents, including elsewhere in Iran, such as the NW Zagros mountains (Jackson & McKenzie 1984) and on the west side of the Lut block (Berberian *et al.* 2001), in California (e.g. Mount & Suppe 1987) and possibly the Himalaya (McCaffrey & Nábělek 1998). Slip partitioning is thus an important mechanism by which oblique convergence is achieved on the continents. McKenzie & Jackson (1983) point out that it is one of the few configurations in which large obliquely convergent strains can be accommodated: most others will require faults to rotate about a vertical axis until they are parallel to the zone boundary, at which point they must either all have the same slip vector as the overall convergence or the orthogonal strike-slip and thrust components must separate on to distinct faults. This evolutionary process is perhaps occurring in the Kopeh Dag today (Figs 4 and 5). Within the range are NW–SE striking right-lateral faults that are oblique to the regional strike and presumably accommodate shortening by rotating anticlockwise, while on its NE margin the strike-slip faulting becomes range-parallel.

4.3 The fate of the Caspian, and its role in the Arabia–Eurasia collision

The South Caspian Basin is an apparently rigid block within an otherwise wide deforming zone from the Persian Gulf to the Caucasus–Kopeh Dag. In this respect it is similar to other aseismic blocks, such as the Dasht-e-Lut in SE Iran (Fig. 1a), the Tarim basin in central Asia (Molnar & Tapponnier 1975), or the central Anatolian plateau (Jackson & McKenzie 1984; McClusky *et al.* 2000), all of which remain essentially undeformed while strain concentrates around their edges. The reasons as to why these blocks are rigid and presumably stronger than their surroundings are not understood and may be different in each example. If the Southern Caspian lithosphere was originally oceanic, it may be relatively strong because of its composition (e.g. Brace & Kohlstedt 1980). Alternatively, if it is thinned continental crust it may be more analogous to the southern Aegean Sea, another low, thin and rigid continental block, which some have suggested may be strong because of its temperature structure (e.g. Sonder & England 1989).

However, the South Caspian Basin has an additional feature that is important: its very low elevation, which is related to its thin and dense (possibly oceanic) crust. It is this feature that causes it to be easily overridden by thrust faults, which is occurring on all sides, and will ultimately cause its complete destruction. Oceanic crust can, in principle, be subducted into the mantle, but this is not an easy process to initiate as it is resisted by forces associated with bending, friction on the subduction interface, and the buoyancy of the crustal part of the subducting lithosphere (e.g. McKenzie 1977; Toth & Gurnis 1998). There are indications of subduction beneath the Apsheron–Balkhan sill, but whether it is still active at the surface is not clear. The low-angle thrusts of the Talesh, so characteristic of oceanic subduction zones, also make this an additional likely site of future subduction. It is easy to see how the South Caspian basement could eventually be consumed by these processes. However, motion of a slab into the mantle only becomes self-sustaining when it reaches a subducted length of $\sim$100 km (McKenzie 1977; Toth & Gurnis 1998), and in neither the Talesh nor the Apsheron–Balkhan sill is there evidence that subduction has reached that stage.

It is also easy to see how a piece of oceanic lithosphere can become isolated and surrounded by continental lithosphere in a collision zone. An example is provided by the eastern Mediterranean (Fig. 12a). In this region, the shortening between Africa and Eurasia is achieved by the westward motion of Turkey away from the collision zone (similar to the westward motion of the South Caspian away from the eastern Alborz and western Kopeh Dag). This westward motion is, in turn, accommodated by thrusting the continental lithosphere of the Aegean over the Mediterranean sea floor in the Hellenic Trench. As a result, the southern Aegean is moving towards Africa at a rate of $\sim$40 mm yr^{-1} (McClusky *et al.* 2000). When the two finally meet, they will have isolated the eastern Mediterranean sea floor as a low (oceanic?) block entirely surrounded by continental lithosphere, resembling in this sense the South Caspian or Black Sea basins. Continued shortening will cause the low-lying block to be overridden by thrusts and eventually consumed. The underlying oceanic basement is likely to be subducted, though the overlying sediments may well be scraped off and attached to the continents. The final result may be an isolated slab with deep earthquakes in an entirely continental mountainous region, with only once-oceanic sediment remaining at the surface to record its origin. The Hindu Kush deep seismic zone is an example of such a slab (Fig. 12b), and may be an indication of the ultimate fate of the South Caspian basement. Furthermore, if subduction occurs, or is attempted, in more than one different direction, as it may be under the Talesh and the Apsheron–Balkhan sill in the Southern Caspian, the final result will be a distorted or twisted slab, such as that seen in the Hindu Kush (e.g. Pegler & Das 1998). Thus we see the isolation and consumption of small oceanic basins in collision zones as a natural consequence of the very 3-D nature of continental tectonics, as exemplified in the eastern Mediterranean.

5 CONCLUSIONS

The South Caspian Basin is an important element in the Arabia–Eurasia collision, being a low, apparently rigid, block being overthrust by continental material on all sides. Its origin remains uncertain: it is either a remnant piece of oceanic lithosphere with unusually thick crust or stretched continental crust with unusually high velocity. The propagation characteristics of S_n and L_g waves and its apparent subduction beneath the northern Caspian, revealed by earthquakes to depths of $\sim$80 km, suggests an oceanic nature for at least part of it. The margins of the Caspian produce a bewildering variety of earthquake focal mechanisms and depths, revealing strike-slip, high- and low-angle thrusting, and normal faulting. It is an important lesson of this study that the simple tectonic patterns contained within this variety could not have been revealed by examination of the routinely published catalogues of locations and CMT solutions, mainly because the depths in those catalogues are too inaccurate. Those patterns are, however, clear when the depths and mechanisms are improved by long-period waveform modelling. From an examination of the active faulting around its margins we estimate that the South Caspian Basin has a westward component of motion relative to both Eurasia and Iran and that this enhances its underthrusting beneath the Talesh mountains in the west. Probable velocities for the South Caspian Basin are about 8–10 mm yr^{-1} to the NW or NNW relative to Eurasia and 13–17 mm yr^{-1} to the SW relative to Iran. Our attempts to reconcile the present-day motions with the geology and geomorphology suggest to us that the current tectonic pattern in the region is young: possibly dating from about 3.4 Ma and triggered by the final closure of minor basins within Iran and the onset of shortening in the Simple Folded Belt of the Zagros mountains. The South Caspian Basin is now being destroyed by underthrusting on its western and northern margins and may ultimately become a twisted slab in the upper mantle, similar to that beneath the Hindu Kush today.

ACKNOWLEDGMENTS

We thank M. Khorehie and M. Qorashi of the Geological Survey of Iran for their constant support of our research in Iran over many years. MA thanks the Geology Institute of Azerbaijan for supporting his fieldwork in the Talesh and Caucasus, and the oil companies who have supported CASP's work in SW Asia. We thank T. Mamedov for providing the Azerbaijan seismic network's locations of the earthquakes near

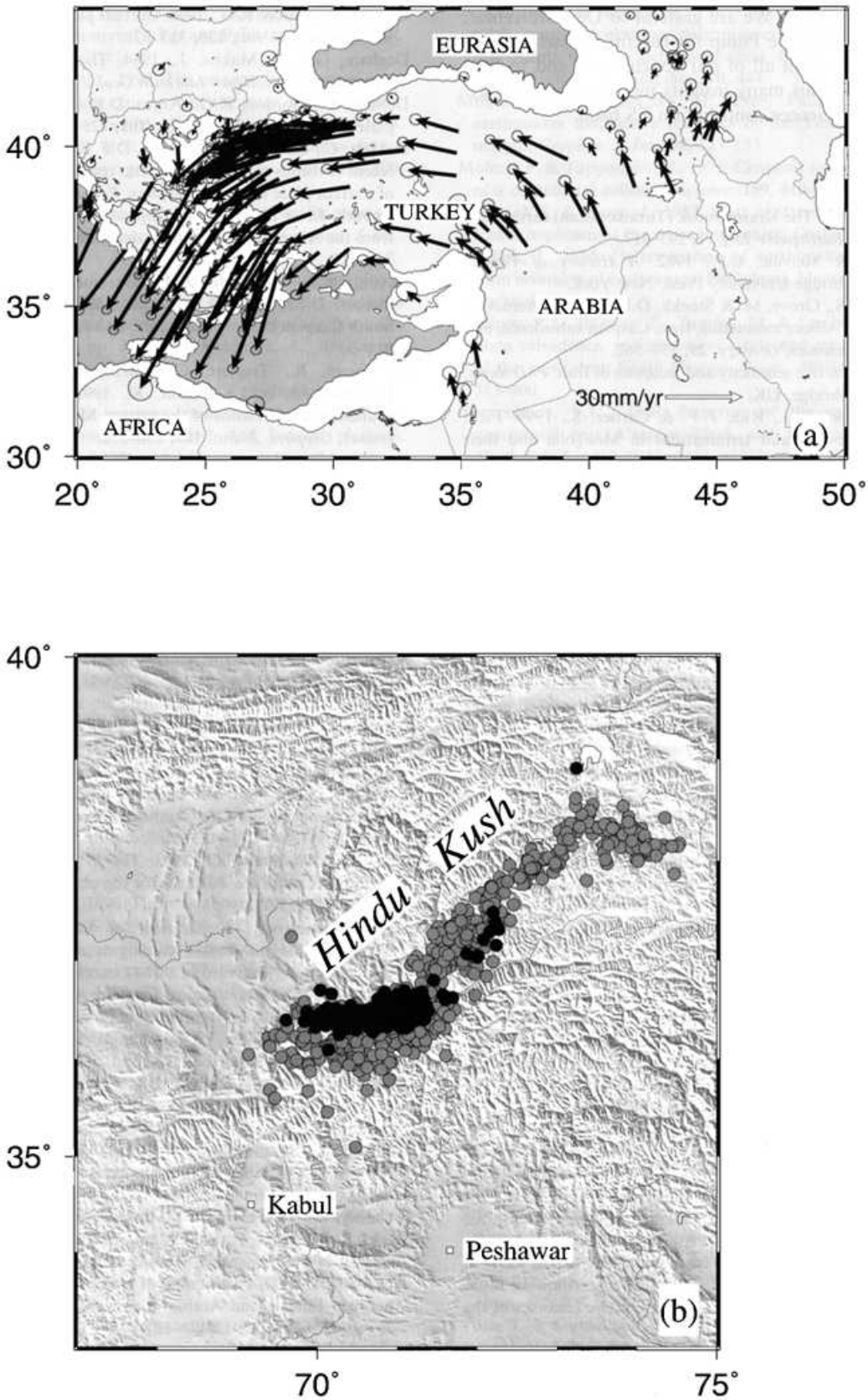

Figure 12. (a) GPS velocities in the eastern Mediterranean region relative to stable Eurasia, from McClusky *et al.* (2000). Bathymetry deeper than 2000 m is in grey. Note how the continued anticlockwise rotation of Turkey and SW motion of Greece will eventually isolate the eastern Mediterranean basin and surround it by continental material. (b) Earthquake epicentres in the depth range 100–200 km (grey) and deeper than 200 km (black) in the Hindu Kush. Data are from the catalogue of Engdahl *et al.* (1998) in the period 1964–1998. Note that in the west the slab defined by the earthquakes dips N, but in the east it dips SE (see also Pegler & Das 1998).

Baku in 2000 November. We are grateful to Dan McKenzie, Denis Hatzfeld and Hervé Philip for careful reviews, though they may not agree with all of our conclusions, and to Rod Graham for sharing his many insights into Caspian geology. Cambridge Earth Sciences contribution ES 6800.

REFERENCES

Ambraseys, N.N., 1997. The Krasnovodsk (Turkmenistan) earthquake of 8 July 1895, *J. Earthquake Eng.*, **1,** 293–317.

Ambraseys, N.N. & Melville, C.P., 1982. *A History of Persian Earthquakes,* Cambridge University Press, New York.

Axen, G.J., Lam, P.S., Grove, M. & Stockli, D.F., 2001. Exhumation of the west-central Alborz mountains, Iran, Caspian subsidence, and collision-related tectonics, *Geology,* **29,** 559–562.

Baker, C., 1993. The active seismicity and tectonics of Iran. *PhD thesis,* University of Cambridge, UK.

Bayasgalan, A., Jackson, J., Ritz, J.-F. & Cartier, S., 1999. Field examples of strike-slip fault terminations in Mongolia and their tectonic significance, *Tectonics,* **18,** 394–411.

Berberian, M., 1976. Contribution to the seismotectonics of Iran (Part II), *Geol. Survey Iran,* Report no. 39.

Berberian, M., 1981. Active faulting and tectonics of Iran, in *Zagros–Hindu Kush–Himalaya Geodynamic Evolution,* pp. 33–69, eds Gupta, H.K. & Delany, F.H., Am. Geophys. Union, Geodynamics Series, Vol. 3.

Berberian, M., 1983. The southern Caspian: a compressional depression floored by a trapped, modified oceanic crust, *Canad. J. Earth Sci.*, **20,** 163–183.

Berberian, M., 1997. Seismic sources of the transcaucasian historical earthquakes, in *Historical and Prehistorical Earthquakes in the Caucasus,* pp. 233–311, eds Giardini, D. & Balassanian, S., Kluwer Academic Publishers, Dordrecht.

Berberian, M. & King, G.C.P., 1981. Towards a paleogeography and tectonic evolution of Iran, *Canadian J. Earth Sci.*, **18,** 210–265.

Berberian, M. & Yeats, R.S., 1999. Patterns of historical earthquake rupture in the Iranian plateau, *Bull. seism. Soc. Am.,* **89,** 120–139.

Berberian, M. & Yeats, R.S., 2001. Contributions of archeological data to studies of earthquake history in the Iranian Plateau, *J. Struct. Geol.,* **23,** 563–584.

Berberian, M., Qorashi, M., Arzhang-Ravesh, B. & Mohajer-Ashjai, A., 1985. Recent tectonics, seismotectonics and earthquake-fault hazard study of the Greater Tehran area. Contribution to the Seismotectonics of Iran, Part V, *Geol. Surv. Iran,* **56,** 316pp. (in Persian).

Berberian, M., Qorashi, M., Jackson, J.A., Priestley, K. & Wallace, T., 1992. The Rudbar–Tarom earthquake of 20 June 1990 in NW Persia: preliminary field and seismological observations, and its tectonic significance, *Bull. seism. Soc. Am.,* **82,** 1726–1755.

Berberian, M., Qorashi, M., Shoja-Taheri, J. & Talebian, M., 1996. Seismotectonic and earthquake-fault hazard investigations in the Semnan region. Contribution to the Seismotectonics of Iran, Part VII, *Geol. Surv. Iran,* **63,** 277pp. (in Persian).

Berberian, M., Jackson, J.A., Fielding, E., Parsons, B.E., Priestley, K., Qorashi, M., Talebian, M., Walker, R., Wright, T.J. & Baker, C., 2001. The 14 March 1998 Fandoqa earthquake (M_w 6.6) in Kerman province, S.E. Iran: re-rupture of the 1981 Sirch earthquake fault, triggering of slip on adjacent thrusts, and the active tectonics of the Gowk fault zone, *Geophys. J. Int.,* **146,** 371–399.

Brace, W.F. & Kohlstedt, D.L., 1980. Limits on lithostatic stress imposed by laboratory experiments, *J. geophys. Res.,* **85,** 6248–6252.

Buday, T., 1980. *The Regional Geology of Iraq: Vol. 1, Stratigraphy and Paleogeography,* Iraq State Organization for minerals, Baghdad, 445pp.

Campos, J., Madariaga, R., Nábělek, J., Bukchin, B.G. & Deschamps, A., 1994. Faulting process of the 1990 June 20 Iran earthquake from broad-band records, *Geophys. J. Int.,* **118,** 31–46.

Chu, D. & Gordon, R.G., 1998. Current plate motions across the Red Sea, *Geophys. J. Int.,* **135,** 313–328.

Deghani, G.A. & Makris, J., 1984. The gravity field and crustal structure of Iran, *Neues Jahrbuch Geol. Paleont. Abh.,* **168,** 215–229.

DeMets, C., Gordon, R.G., Argus, D.F. & Stein, S., 1990. Current plate motions, *Geophys. J. Int.,* **101,** 425–478.

DeMets, C., Gordon, R.G., Argus, D.F. & Stein, S., 1994. Effects of recent revisions to the geomagnetic reversal time scale on estimates of current plate motions, *Geophys. Res. Lett.,* **21,** 2191–2194.

Dercourt, J., *et al.*, 1986. Geological evolution of the Tethys belt from the Atlantic to the Pamirs since the Lias, *Tectonophysics,* **123,** 241–315.

Devlin, W.J., Cogswell, J.M., Gaskins, G.M., Isaksen, G.H., Pitcher, D.M., Puls, D.P., Stanley, K.O. & Wall, G.R.T., 1999. South Caspian basin: young, cool, and full of promise, *GSA Today,* **9,** 1–9.

de Voogd, B., Truffert, C., Chamot-Rooke, N., Huchon, P., Lallemant, S. & Le Pichon, X., 1992. Two-ship deep seismic soundings in the basins of the eastern Mediterranean Sea (Pasiphae cruise), *Geophys. J. Int.,* **109,** 536–552.

Dewey, J.F., Hempton, M.R., Kidd, W.S.F., Şaroğlu, F. & Şengör, A.M.C., 1986. Shortening of continental lithosphere: the neotectonics of Eastern Anatolia—a young collision zone, in *Collision tectonics,* pp. 3–36, eds Coward, M.P. & Ries, A.C., *Geol. Soc. Spec. Publ. London,* Vol. 19.

Engdahl, E.R., van der Hilst, R. & Buland, R., 1998. Global teleseismic earthquake relocation with improved travel times and procedures for depth determination, *Bull. seism. Soc. Am.,* **88,** 722–743.

Falcon, N.L., 1969. Problems of the relationship between surface structure and deep displacements illustrated by the Zagros range, in *Time and Place in Orogeny,* pp. 9–22, *Geol. Soc. Spec. Publ. London,* Vol. 3.

Falcon, N.L., 1974. Southern Iran: Zagros mountains, in *Mesozoic–Cenozoic Orogenic Belts: Data for Orogenic Studies,* pp. 199–211, ed. Spencer, A., *Geol. Soc. Spec. Publ. London,* Vol. 4.

Fitch, T.J., 1972. Plate convergence, transcurrent faults and internal deformation adjacent to southeast Asia and the western Pacific, *J. Geophys. Res.*, **77,** 4432–4460.

Gao, L. & Wallace, T.C., 1995. The 1990 Rudbar–Tarom Iranian earthquake sequence: evidence for slip partitioning, *J. geophys. Res.*, **100,** 15 317–15 332.

Harvard University, Department of Geological Sciences, 2000. Centroid Moment Tensor catalogue, available online at: http://www.seismology.harvard.edu/CMTsearch.html

Hempton, M.R., 1987. Constraints on Arabian plate motion and extensional history of the Red Sea, *Tectonics,* **6,** 687–705.

Hessami, K.T., Alyasin, S. & Jamalih, F., 1997. An investigation of some historical earthquakes and paleoseismic sources in Iran, in *Historical and Prehistorical Earthquakes in the Caucasus,* pp. 189–199, eds Giardini, D. & Balassanian, S., Kluwer Academic Publishers, Dordrecht.

Hinds, D.J., Simmons, M.D., Allen, M.B. & Aliyeva, E., 2001. Architecture variability within the Pereriva and Balakhany suites of the Neogene Productive Series, Azerbaijan: implications for reservoir quality. *Am. Assoc. Petrol. Geol. Memoir,* in press.

Isacks, B. & Molnar, P., 1969. Mantle earthquake mechanisms and the sinking of the lithosphere, *Nature,* **223,** 1121–1124.

Jackson, J.A, 1992. Partitioning of strike-slip and convergent motion between Eurasia and Arabia in eastern Turkey and the Caucasus, *J. geophys. Res.*, **97,** 12 471–12 479.

Jackson, J.A. & Ambraseys, N.N., 1997. Convergence between Eurasia and Arabia in eastern Turkey and the Caucasus, in *Historical and Prehistorical Earthquakes in the Caucasus,* pp. 79–90, eds Giardini, D. & Balassanian, S., Kluwer Academic Publishers, Dordrecht.

Jackson, J.A. & Fitch, T.J., 1979. Seismotectonic implications of relocated aftershock sequences in Iran and Turkey, *Geophys. J. R. astr. Soc.*, **57,** 209–229.

Jackson, J.A. & McKenzie, D.P., 1984. Active tectonics of the Alpine–Himalayan belt between western Turkey and Pakistan, *Geophys. J. R. astr. Soc.*, **77,** 185–264.

Jackson, J.A. & McKenzie, D., 1988. The relationship between plate motions and seismic moment tensors, and the rates of active deformation in the Mediterranean and Middle East, *Geophys. J.*, **93,** 45–73.

Jackson, J.A., Haines, A.J. & Holt, W.E., 1995. The accommodation of Arabia–Eurasia plate convergence in Iran, *J. geophys. Res.*, **100,** 15 205–15 219.

Jestin, F., Huchon, P., & Gaulier, J.M., 1994. The Somalia plate and the East African rift system: present-day kinematics, *Geophys. J. Int.*, **116,** 637–654.

Jones, R.W. & Simmons, M.D., 1997. A review of the stratigraphy of eastern Paratethys (Oligocene–Holocene), with particular emphasis on the Black Sea, in *Regional and Petroleum Geology of the Black Sea and Surrounding Regions,* pp. 39–52 ed. Robinson, A., *Am. Assoc. Petrol. Geol. Memoir,* Vol. 68.

Kadinsky-Cade, K., Barazangi, M., Oliver, J. & Isacks, B., 1981. Lateral variations of high-frequency seismic wave propagations at regional distances across the Turkish and Iranian plateaus, *J. geophys. Res.*, **86,** 9377–9396.

Karakhanian, A.S., Djrbashian, R.T., Trifonov, V.G., Philip, H. & Ritz, J.F., 1997. Active faults and strong earthquakes of the Armenian upland, in *Historical and Prehistorical Earthquakes in the Caucasus,* pp. 181–187, eds Giardini, D. & Balassanian, S., Kluwer Academic Publishers, Dordrecht.

Kopp, M.L., 1997. *Lateral escape structures in the Alpine–Himalayan Collision Belt,* ed. Leonov Yu.G., Russian Academy of Sciences, Geological Institute, Transactions, vol. 506 (in Russian), Scientific World, Moscow, 312pp.

Lyberis, N. & Manby, G., 1999. Oblique to orthogonal convergence across the Turan block in the post-Miocene, *Am. Assoc. Petroleum Geologists Bull.*, **83,** 1135–1160.

Maggi, A., Jackson, J.A., McKenzie, D. & Priestley, K., 2000a. Earthquake focal depths, effective elastic thickness, and the strength of the continental lithosphere, *Geology,* **28,** 495–498.

Maggi, A., Jackson, J.A., Priestley, K. & Baker, C., 2000b. A re-assessment of focal depth distributions in southern Iran, the Tien Shan and northern India: do earthquakes really occur in the continental mantle?, *Geophys. J. Int.*, **143,** 629–661.

Mangino, S. & Priestley, K., 1998. The crustal structure of the southern Caspian region, *Geophys. J. Int.*, **133,** 630–648.

McCaffrey, R., 1992. Oblique plate convergence, slip vectors, and forecarc deformation, *J. geophys. Res.*, **97,** 8905–8915.

McCaffrey, R. & Abers, G., 1988. SYN3: a program for inversion of teleseismic body waveforms on microcomputers, *Air Force Geophysics Laboratory Technical report, AFGL-TR-88-0099,* Hanscomb Air Force Base, Ma.

McCaffrey, R. & Nábělek, J., 1987. Earthquakes, gravity and the origin of the Bali basin: an example of a nascent continental fold-and-thrust belt, *J. geophys. Res.*, **92,** 441–460.

McCaffrey, R. & Nábělek, J., 1998. Role of oblique convergence in the active deformation of the Himalayas and southern Tibet plateau, *Geology,* **26,** 691–694.

McCaffrey, R., Zwick, P. & Abers, G., 1991. SYN4 Program, *IASPEI Software Library,* **3,** 81–166.

McCall, G.J.H., 1996. The inner Mesozoic to Eocene ocean of south and central Iran and associated microcontinents, *Geotectonics,* **29,** 490–499.

McClusky, S., *et al.*, 2000. GPS constraints on plate motions and deformations in the Eastern Mediterranean: implications for plate dynamics, *J. geophys. Res.*, **105,** 5695–5719.

McKenzie, D., 1972. Active tectonics of the Mediterranean region, *Geophys. J. R. astr. Soc.*, **30,** 109–185.

McKenzie, D., 1977. The initiation of trenches: a finite amplitude instability, in *Island Arcs, Deep Sea Trenches, and Back-arc Basins,* pp. 57–61, eds Talwani, M. & Pitman, W.C., Maurice Ewing Series, Vol. 1, Am. Geophys. Union.

McKenzie, D. & Jackson, J., 1983. The relationship between strain rates, crustal thickening, paleomagnetism, finite strain and fault movements within a deforming zone, *Earth planet. Sci. Lett.*, **65,** 182–202, and correction *ibid.*, **70,** 444.

Molnar, P. & Lyon-Caen, H., 1989. Fault plane solutions of earthquakes and active tectonics of the Tibetan Plateau and its margin, *Geophys. J. Int.*, **99,** 123–153.

Molnar, P. & Tapponnier, P., 1975. Cenozoic tectonics of Asia: effects of a continental collision, *Science,* **189,** 419–425.

Mount, V.S. & Suppe, J., 1987. State of stress near the San Andreas Fault: implications for wrench tectonics, *Geology,* **15,** 1143–1146.

Nábělek, J., 1984. Determination of earthquake source parameters from inversion of body waves, PhD thesis, Massachusetts Institute of Technology.

Nadirov, R.S., Bagirov, E., Tagiyev, M. & Lerche, I., 1997. Flexural plate subsidence, sedimentation rates, and structural development of the super-deep South Caspian Basin, *Marine Petrol. Geol.*, **14,** 383–400.

Neprochnov, Y.U., 1968. Structure of the earth's crust of epi-continental seas: Caspian Black and Mediterranean, *Canad. J. Earth Sci.*, **5,** 1037–1043.

Okay, A.I., Şengör, A.M.C. & Görür, N., 1994. Kinematic history of the opening of the Black Sea and its effect on the surrounding regions, *Geology,* **22,** 267–270.

Pegler, G. & Das, S., 1998. An enhanced image of the Pamir–Hindu Kush seismic zone from relocated earthquake hypocentres, *Geophys. J. Int.*, **134,** 573–595.

Philip, H., Cisternas, A., Gvishiani, A. & Gorshkov, A., 1989. The Caucasus: an actual example of the initial stages of continental collision, *Tectonophysics,* **161,** 1–21.

Priestley, K., Baker, C. & Jackson, J., 1994. Implications of earthquake focal mechanism data for the active tectonics of the South Caspian Basin and surrounding regions, *Geophys. J. Int.*, **118,** 111–141.

Priestley, K. & Patton, H., 2001. Shear wave structure of the South Caspian lithosphere, *Bull. seism. Soc. Am.*, in press.

Reynolds, A.D. *et al.*, 1998. Implications of outcrop geology for reservoirs in the Neogene Productive Series, Apsheron peninsula, Azerbaijan, *Am. Assoc. Petroleum Geologists Bull.*, **82,** 25–49.

Rezanov, I.A. & Chamo, S.S., 1969. Reasons for absence of a 'granitic' layer in basins of the South Caspian and Black Sea type, *Canad. J. Earth Sci.*, **6,** 671–678.

Rustanovich, D.N. & Shirakova, E.I., 1964. Some results of a study of the Ashkabad earthquake of 1948, *Izv. Akad. Nauk. USSR, Ser. Geophiz.*, 1077–1080.

Şengör, A.M.C., 1990. A new model for the late Paleozoic–Mesozoic tectonic evolution of Iran and implications for Oman, in *The Geology and tectonics of the Oman region, Geol. Soc. Spec. Publ. London,* **49,** 797–831.

Shikalibeily, E.Sh. & Grigoriants, B.V., 1980. Principal features of the crustal structure of the south-Caspian basin and the conditions of its formation, *Tectonophysics,* **69,** 113–121.

Sonder, L. & England, P.C, 1989. Effects of temperature-dependent rheology on large-scale continental extension, *J. geophys. Res.*, **94,** 7603–7619.

Stöcklin, J., 1974. Northern Iran: Alborz mountains, in *Mesozoic–Cenozoic Orogenic Belts: Data for Orogenic Studies,* pp. 213–234, ed. Spencer, A., *Geol. Soc. Spec. Publ. London,* Vol. 4.

Tchalenko, J.S., 1975. Seismicity and structure of the Kopet Dagh (Iran, U.S.S.R.), *Phil. Trans. R. Soc. London Ser. A,* **278A,** 1–28.

Toth, J. & Gurnis, M., 1998. Dynamics of subduction initiation at preexisting fault zones, *J. geophys. Res.*, **103,** 18 053–18 067.

Trifonov, V.G., 1978. Late Quaternary tectonic movements of western and central Asia, *Geol. Soc. Am. Bull.*, **89,** 1059–1072.

Trifonov, V.G., Vostrikov, G.A., Lykov, V.I., Orazsakhatov, K. & Skobelev, S.F., 1986. Tectonic aspects of the 1983 Kum-Dag earthquake, west Turkmenia, *Int. Geol. Review,* 377–389.

Wellman, H.W., 1966. Active wrench faults of Iran, Afghanistan and Pakistan, *Geol. Rundschau,* **55,** 716–735.

White, R.S., McKenzie, D. & O'Nions, R.K., 1992. Oceanic crustal thickness from seismic measurements and rare earth element inversions, *J. geophys. Res.*, **97,** 19 683–19 715.

Wright, T.J., Parsons, B.E., Jackson, J.A., Haynes, M., Fielding, E.J., England, P.C. & Clarke, P.J., 1999. Source parameters of the 1 October 1995 Dinar (Turkey) earthquake from SAR interferometry and seismic bodywave modelling, *Earth planet. Sci. Lett.*, **172,** 23–37.

Zonenshain, L.P. & Le Pichon, X., 1986. Deep basins of the Black Sea and Caspian Sea as remnants of Mesozoic back-arc basins, *Tectonophysics,* **123,** 181–211.

Zwick, P., McCaffrey, R. & Abers, G., 1994. MT5 Program, *IASPEI Software Library,* **4.**

APPENDIX A: WAVEFORM MODELLING OF EARTHQUAKES

This appendix contains the results of long-period *P* and *SH* waveform analysis carried out for the earthquakes marked A in the final column of Table 1 and those marked * and † in the penultimate column of Table 2.

There are two formats of figure used in this appendix. The format of Fig. A2 shows *P* (top) and *SH* (bottom) observed (solid) and synthetic (dashed) waveforms for the solutions in Tables 1 or 2, which usually correspond to the final inversion result, or the 'minimum-misfit' solution. Station positions on the *P* (top) and *SH* (bottom) focal spheres are identified by capital letters and arranged clockwise starting from north. STF is the source time function. Vertical ticks on the seismograms indicate the inversion window. Numbers beneath the header line are strike, dip, rake, centroid depth (km), and moment (N m). Stations were weighted according to azimuthal density and then the S seismogram weights were halved, to compensate for their larger amplitudes. Comments appropriate to individual earthquakes are given in the figure captions.

The second type of format is that of Fig. A1. This shows several lines of observed (solid) and synthetic (dashed) seismograms at particular stations, each line corresponding to a solution where strike/dip/rake/depth/M_0 is given in the header above the *P* (left) and *SH* (right) focal spheres on the left. The purpose of this kind of figure is to demonstrate the sensitivity of the waveforms to a particular source parameter (usually depth), in cases where there were insufficient waveforms to carry out a full inversion for all source parameters of the sort displayed in Fig. A1. An explanation of each line of waveforms is given in the individual figure captions.

Synthetic seismograms for all earthquakes with centroid depths <30 km were calculated in a half-space with V_p= 6.5 km s^{-1}, V_s=3.7 km s^{-1} and density (ρ) 2.8 Mgm m^{-3}. Synthetic seismograms for most of the deeper earthquakes were calculated using a layer with V_p=6.5 km s^{-1}, V_s=3.7 km s^{-1} and ρ=2.8 Mgm m^{-3} above a half-space of V_p=8.1 km s^{-1}, V_s = 4.7 km s^{-1} and ρ = 3.2 Mgm m^{-3}. The depth of the interface between the layer and half-space is given in the figure captions. For the two earthquakes at 40 and 33 km near Baku in Fig. 6 a special velocity structure was used, described in the captions for Figs. 16A and 17A.

For many of the earthquakes the purpose of the inversion was to constrain or confirm the centroid depth, which is not well determined by the Harvard CMT solutions, especially for shallow events. The simple patterns of seismicity discussed in the main text cannot be seen unless the centroid depths are known with confidence. The corresponding Harvard best-double-couple CMT solutions are given in the figure captions and are often similar in orientation to those determined here. The difference in depth between the solutions is often accompanied by a difference in moment, which might arise from a combination of factors including: (1) a trade-off between depth and M_0 for shallow earthquakes; (2) differences in the velocity models used; (3) a contribution from a non-double-couple component in the Harvard solution; (4) a contribution from poorly resolved M_{xz} and M_{yz} components for shallow earthquakes in the Harvard solution (see Wright *et al.* 1999).

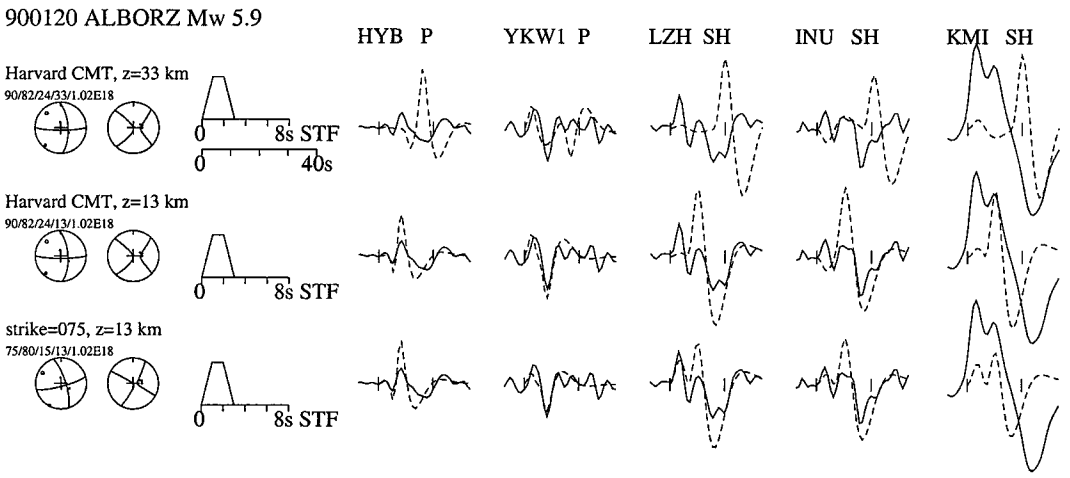

Figure A1. Waveforms for the 1990 January 20 earthquake (M_w 5.9) near Firuzkuh in the eastern Alborz. The interest in this earthquake is in its depth (fixed at 33 km by Harvard) and its location near a prominent ENE–WNW left-lateral strike-slip fault (Figs 7 and 9c). There were insufficient clear waveforms for a full inversion. Line 1 shows two *P* and three *SH* observed (solid) and synthetic (dashed) waveforms corresponding to the Harvard best-double-couple solution at its fixed depth of 33 km and with its E–W left-lateral orientation. The fit of the synthetic *P* waves to the observed *P* seismograms is not good, mainly because, at 33 km, the centroid is too deep. A better fit to the *P* waves is achieved when the centroid is moved to 13 km (line 2), but the fit of the *SH* waveforms remains bad. The *SH* waveforms fit better, particularly at eastern azimuths (LZH, KMI), where a clear double-pulse is seen, when the strike is rotated from 090° to 075° (line 3), which corresponds better to the observed strike of the Firuzkuh fault on the ground (Fig. 9c).

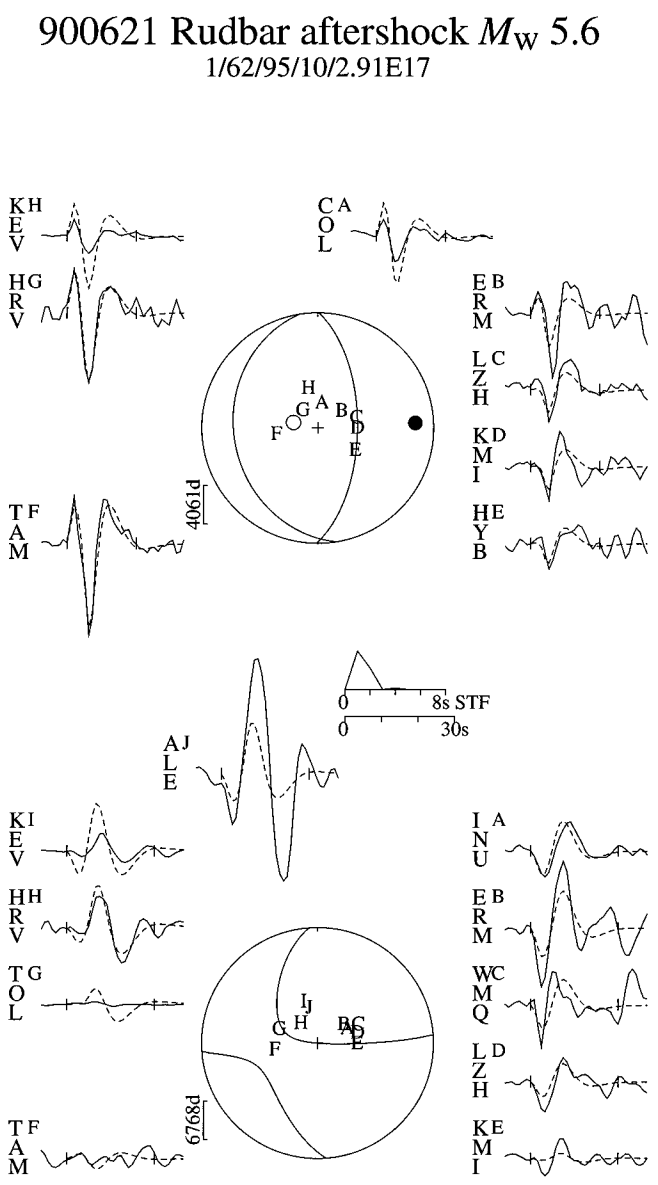

Figure A2. Minimum misfit solution for the earthquake of 1990 June 21 (M_w 5.6), an aftershock of the 1990 June 20 Rudbar–Tarom earthquake (M_w 7.3). This event shows N–S reverse faulting at the end of an E–W left-lateral strike-slip fault (Fig. 7a). Our solution is similar to that of Gao & Wallace (1995), who obtained 023/64/92/8 km/ 4.0×10^{17} N m using a combination of regional and teleseismic waveforms, and similar in orientation to the Harvard CMT best-double-couple solution (351/68/76/15 km (fixed)/4.95×10^{17} N m/53 per cent double-couple).

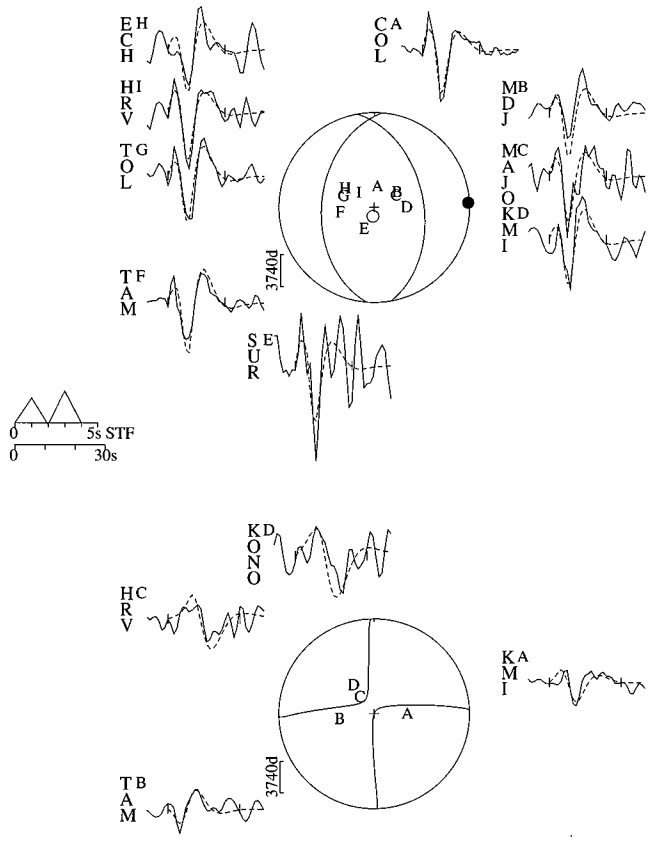

Figure A3. Minimum misfit solution for the earthquake of 28 November 1991 (M_w 5.7), another aftershock of the 1990 June 20 Rudbar–Tarom earthquake (M_w 7.3), and, like that of 21 June 1990 (Fig. A2), one that involved N–S reverse faulting (Fig. 7a). The Harvard CMT best-double-couple solution is similar in orientation (354/63/65/15 km (fixed)/3.24×10^{17} N m/92 per cent double-couple).

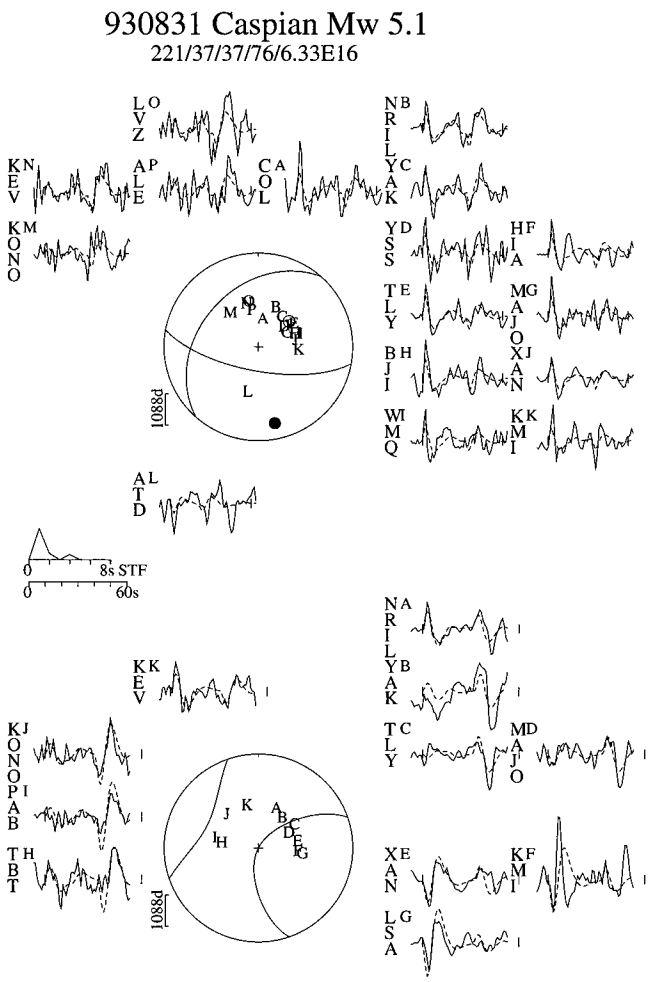

Figure A4. Minimum misfit solution for 31 August 1993 (M_w 5.1) earthquake in the central Caspian. This event has the deepest confirmed centroid in the region, at 76 km, which is well constrained by numerous surface reflections visible on *P* and *SH* records. The Harvard CMT best-double-couple solution is similar to the one shown here (219/39/35/82 km/9.87 × 10^{16} N m/94 per cent double-couple).

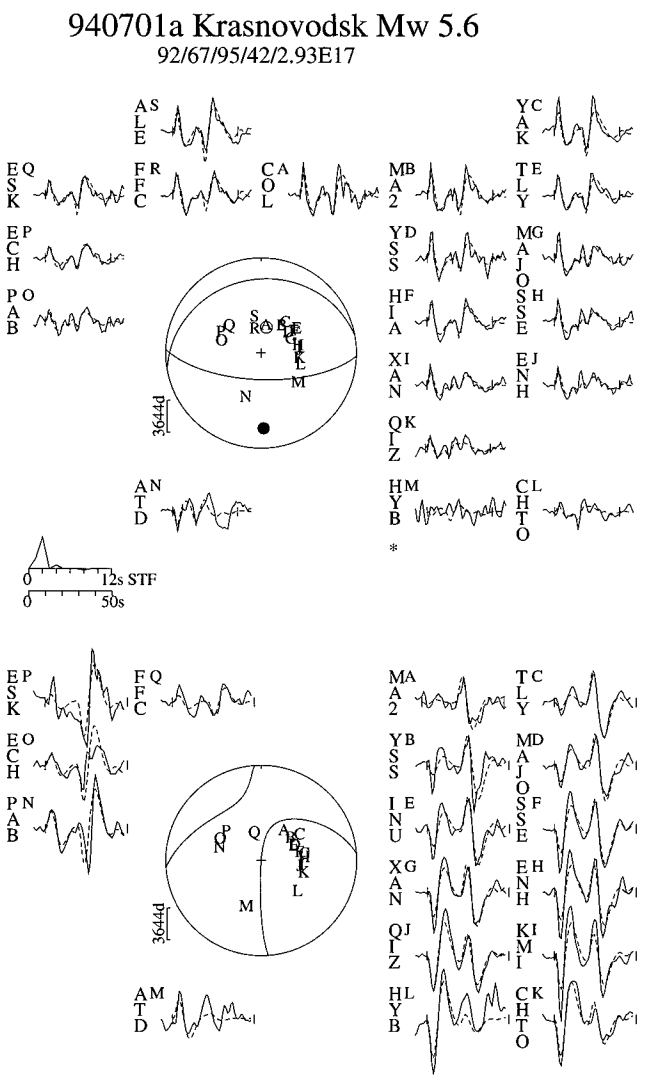

Figure A5. Minimum misfit solution for the first (at 10:12) of two earthquakes on 1 July 1994 near Krasnovodsk in Turkmenistan at ~40 km depth (Fig. 6). The depth is well resolved by the separated direct (*P*, *S*) and reflected (*pP*, *sP*, *sS*) phases at many stations. Synthetics were calculated with the interface separating the layer of V_p 6.5 km s^{-1} from the half-space of V_p 8.1 km s^{-1} at 40 km. This solution is similar to that of the Harvard CMT best-double-couple solution (93/62/101/57 km/3.05 × 10^{17} N m/99 per cent double-couple).

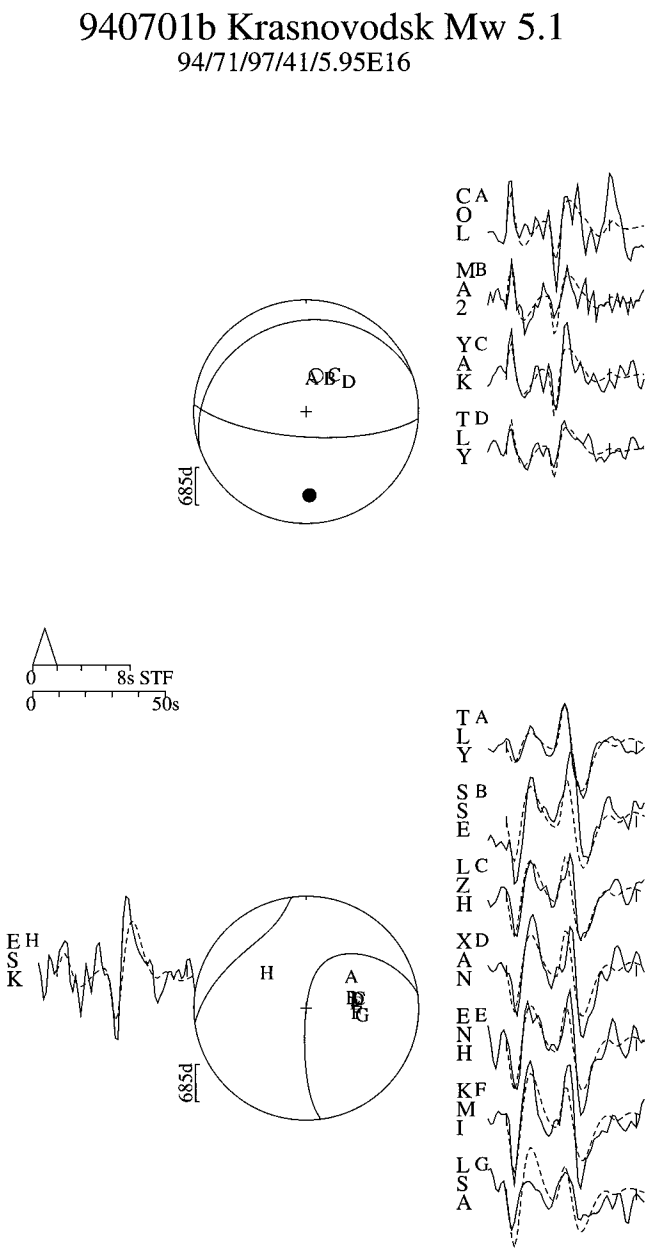

Figure A6. Minimum misfit solution for the second earthquake (at 19:50) on 1 July 1994 near Krasnovodsk, also at ~40 km. As in Fig. A5, the depth is well resolved by the separated direct and reflected phases. Synthetics were calculated in the same velocity structure as for Fig. A5. The Harvard CMT best-double-couple solution is similar in orientation (88/58/78/50 km/7.46 × 10^{16} N m/92 per cent double-couple).

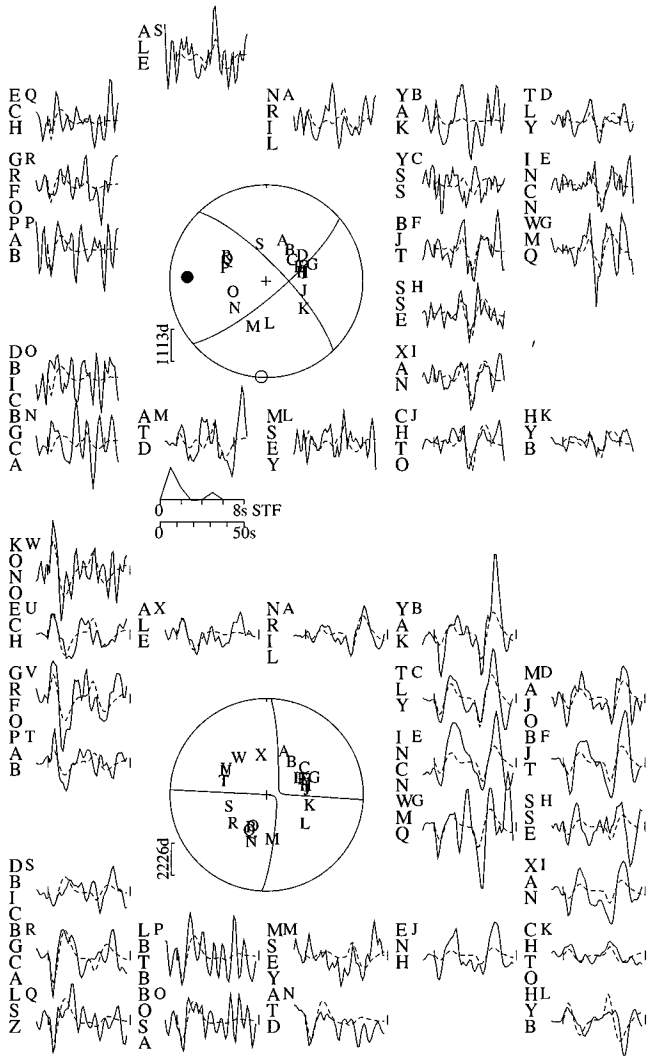

Figure A7. Minimum misfit solution for a deep (~61 km) strike-slip event near the Apsheron–Balkhan sill (Fig. 6). The earthquake was only M_w 5.3 and some waveforms are noisy, as well as quite small in amplitude near nodal planes. Nonetheless, the clear surface reflections in the *P* waves at eastern stations (e.g. SSE, XAN, CHTO) and in the *SH* waves in the NE and SE quadrants (e.g. YAK, TLY, XAN, HYB) constrain the depth to within ~ ±5 km. Synthetics were calculated with the interface between the top layer (V_p 6.5 km s^{-1}) and half-space (V_p 8.1 km s^{-1}) at 30 km, and with a water depth of 500 m. Our solution is similar to that of the Harvard best-double-couple (314/75/-42/26 km/2.15 × 10^{17} N m/57 per cent double-couple) except for the centroid depth, which trades off against moment.

970204a Kopeh Dag M_W 5.4
338/67/150/13/1.61E17

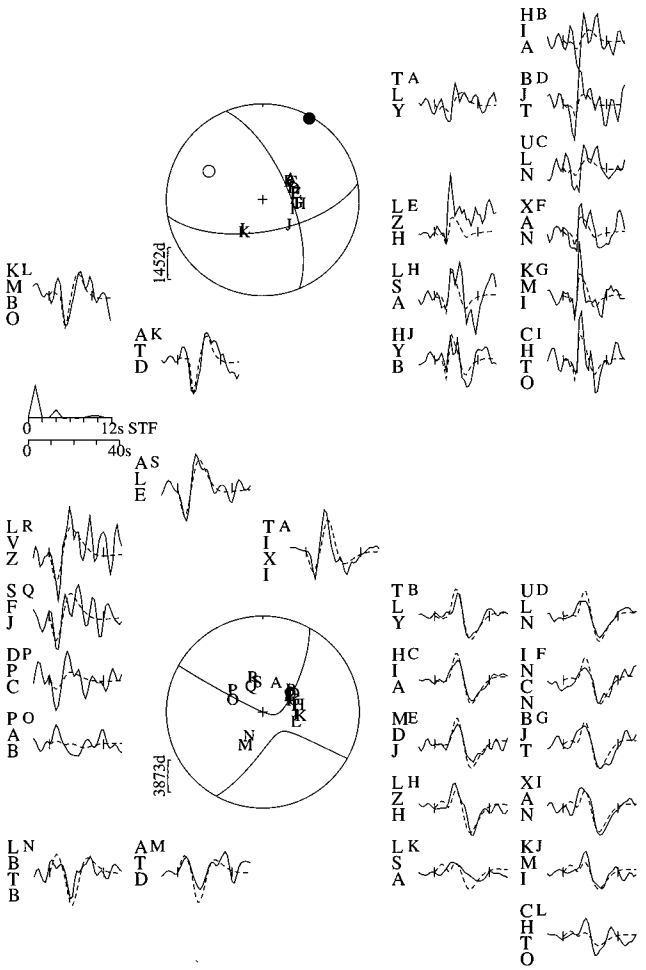

Figure A8. Minimum misfit solution for the first (at 09:53) and smaller (M_w 5.4) of two earthquakes on 1997 February 4 near Bojnurd in the Kopeh Dag. The solution is similar to that of the second event in Fig. A9. The Harvard CMT best-double-couple solution is similar in orientation (342/77/153/15 km (fixed)/1.72×10^{17} N m/92 per cent double-couple).

970204b Kopeh Dag M_W 6.4
326/75/173/8/5.75E18

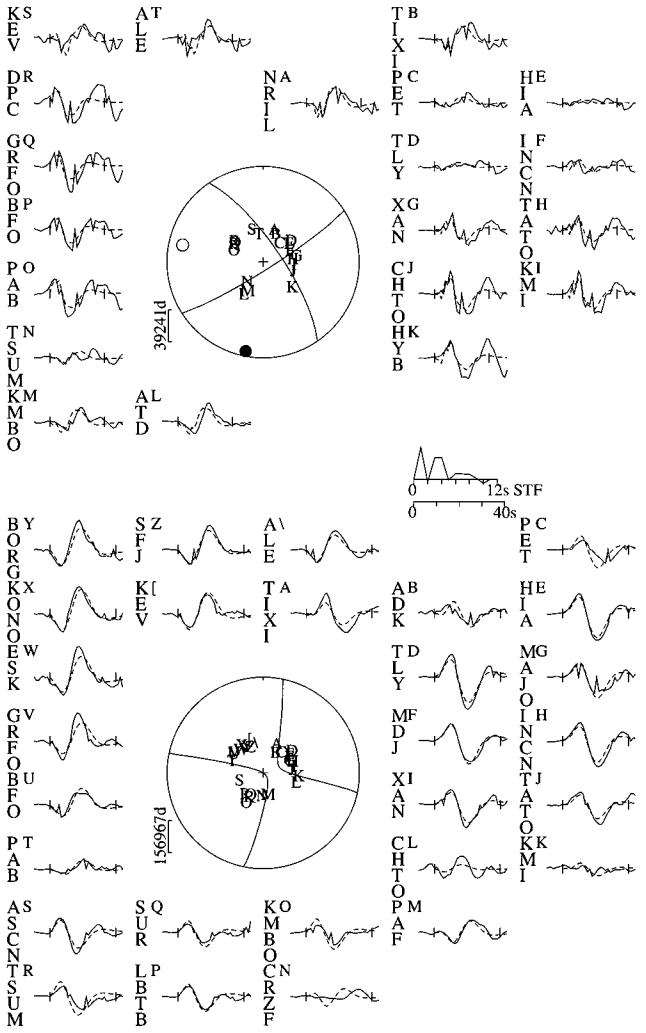

Figure A9. Minimum misfit solution for the second (at 10:37) and larger (M_w 6.4) earthquake on 1997 February 4 near Bojnurd in the Kopeh Dag. The solution is well constrained by the large number of well-distributed waveforms. The Harvard CMT best-double-couple solution is similar in orientation (328/81/−171/15 km (fixed)/6.72×10^{18} N m/96 per cent double-couple). No surface faulting was reported for these two events, but the epicentral area contains well-known NW–SE right-lateral strike-slip faults that are prominent in the landscape and satellite imagery (see Tchalenko 1975).

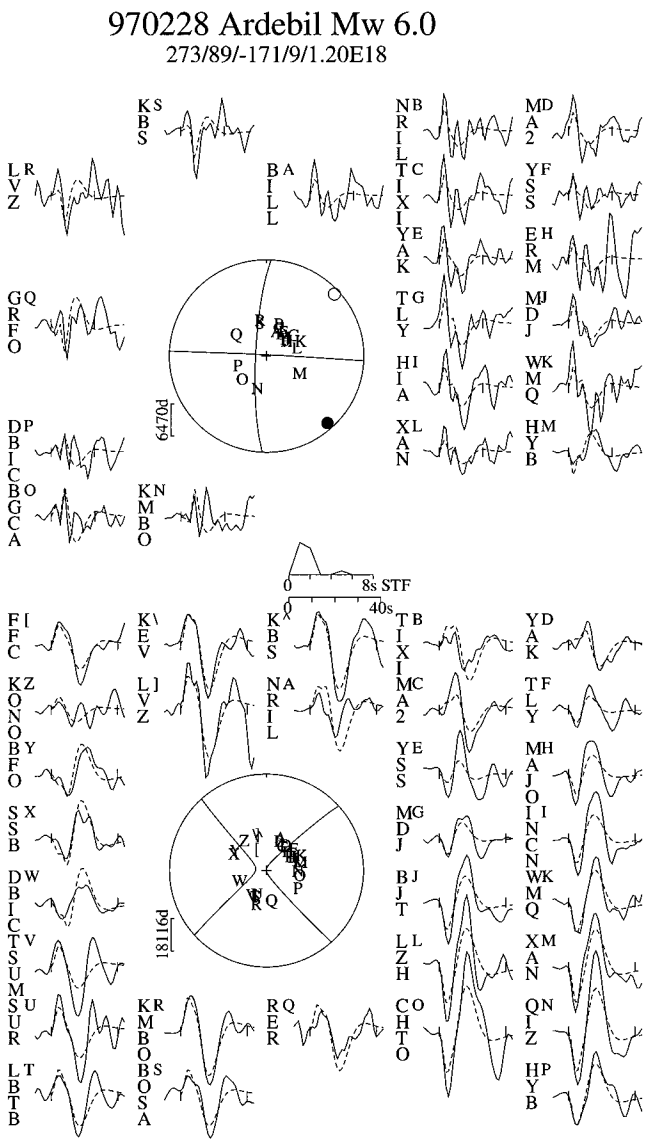

Figure A10. Minimum misfit solution for an earthquake of M_w 6.0 near Ardebil, west of the Talesh, on 1997 February 28. The solution is well constrained by abundant clear waveforms. The Harvard CMT best-double-couple solution is similar in orientation (283/77/−146/15 km (fixed)/1.73×10^{18} N m/79 per cent double-couple). No co-seismic surface faulting was reported, and little is known of the active structures in the epicentral region.

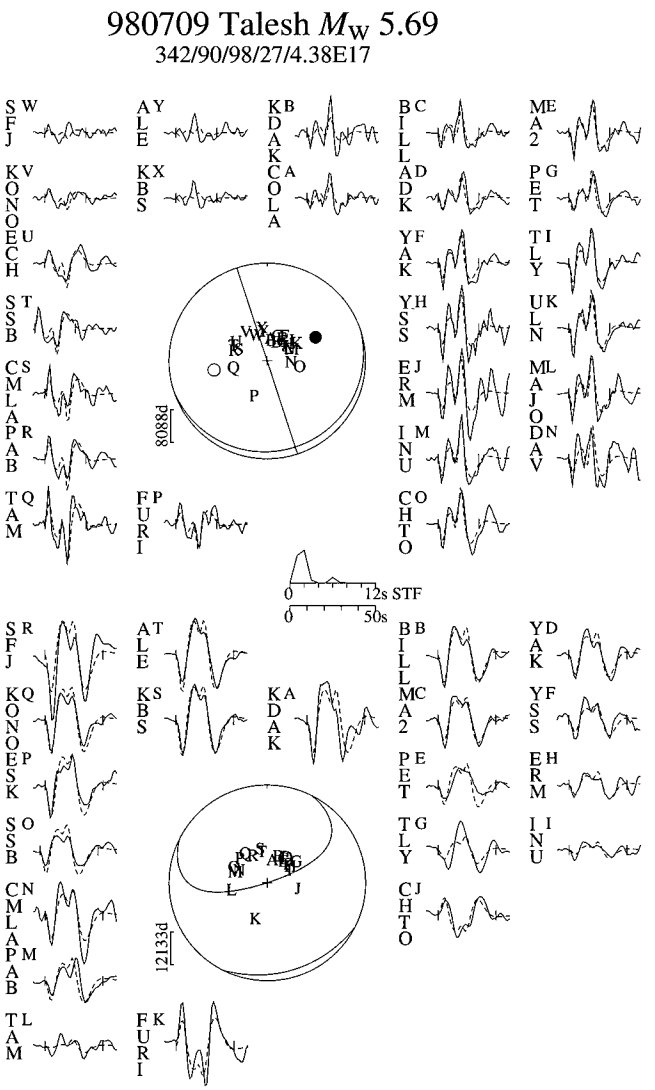

Figure A12. Minimum misfit solution for an earthquake of M_w 5.7 in the Talesh on 9 July 1998. The depth of ~27 km is well constrained by surface reflections on *P* and *SH* records. The Harvard CMT best-double-couple solution is similar in orientation (349/82/90/20 km/ 10.29×10^{17} N m/96 per cent double-couple).

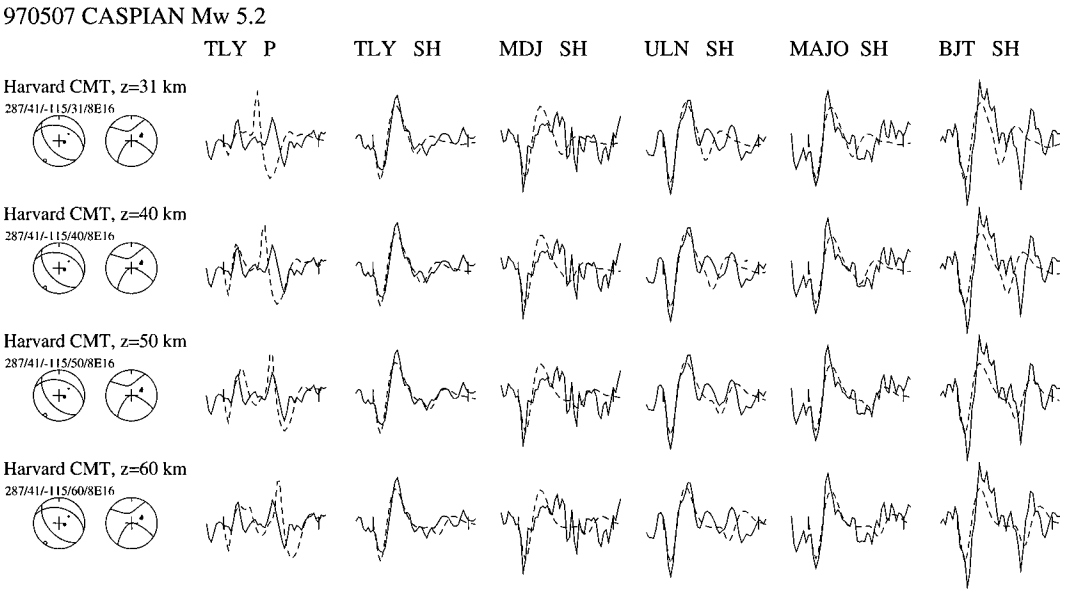

Figure A11. Waveforms for an earthquake of M_w 5.2 on 7 May 1997 on the Apsheron–Balkhan sill (Fig. 6). There were insufficient clear seismograms for a full inversion, but the depth of 50 ± 5 km can be confirmed. The four lines of waveforms show synthetics calculated at 31, 40, 50 and 60 km using the Harvard CMT orientation and M_0 with a short (2 s) impulsive time function. The interface between the top layer (V_p 6.5 km s^{-1} and the half-space of V_p 8.1 km s^{-1} was at 30 km and a water depth of 500 m was included. Particularly clear surface reflections are seen at TLY (*P*) and BJT (*SH*). The Harvard depth was 63 km (58 per cent double-couple).

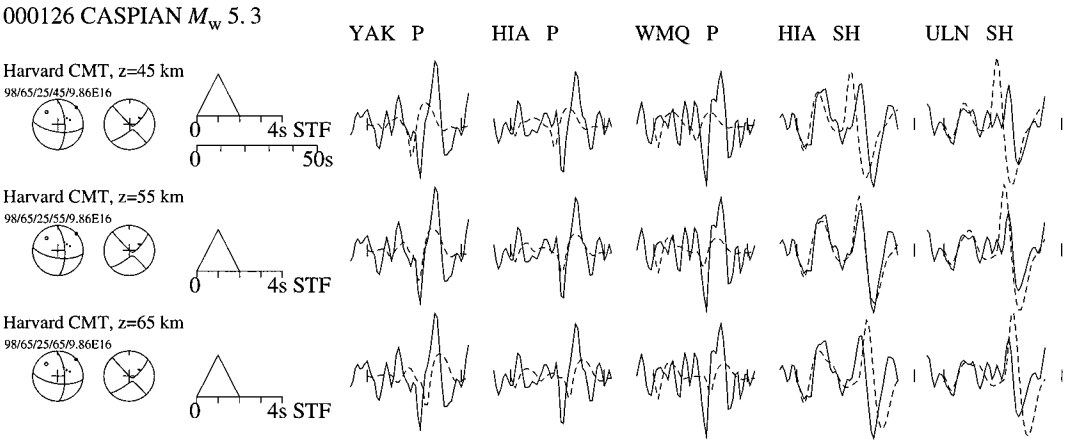

Figure A13. Waveforms for an earthquake of M_w 5.3 on 26 January 2000 on the Apsheron–Balkhan sill (Fig. 6). There were insufficient clear seismograms for a full inversion, but the depth of 55 ± 5 km can be confirmed. The three lines of waveforms show synthetics calculated at 45, 55 and 65 km using the Harvard CMT orientation and M_0 with a short (2 s) impulsive time function. The interface between the top layer (V_p 6.5 km s^{-1} and the half-space of V_p 8.1 km s^{-1} was at 30 km. Particularly clear surface reflections are seen at all the records shown here. The Harvard depth was 65 km (70 per cent double-couple).

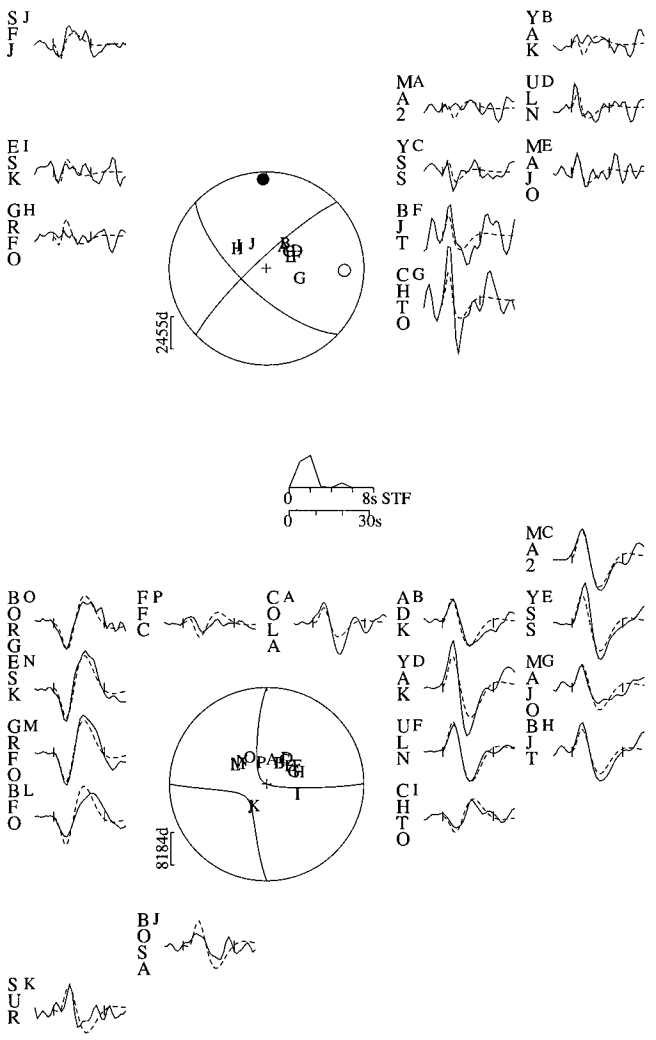

Figure A14. Minimum misfit solution for an earthquake of M_w 5.6 in the Kopeh Dag on 22 August 2000. The Harvard CMT best-double-couple solution is similar in orientation (133/80/-179/33 km (fixed)/ 4.6×10^{17} N m/100 per cent double-couple).

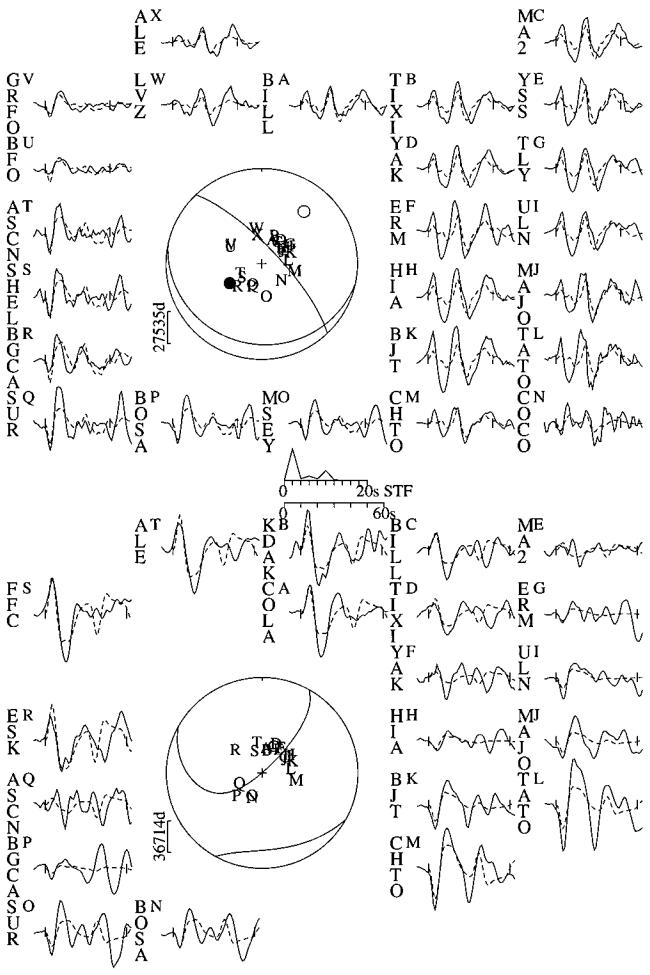

Figure A15. Minimum misfit solution for the first of two earthquakes near Baku on 25 November 2000, this one at 18:09 GMT and with M_w 6.2. This is an area of the South Caspian Basin where the sediment thickness is known to be great, overpressured and with low velocity. We used a velocity model involving a layer 20 km thick with $V_p = 4.0$ km s^{-1}, $V_s = 2.3$ km s^{-1} and density (ρ) 2.3 Mgm m^{-3} above a half-space of $V_p = 6.5$ km s^{-1}, $V_s = 3.7$ km s^{-1} and density (ρ) 2.8 Mgm m^{-3}. The depth is reasonably well-constrained by the surface-reflected phases, with some uncertainty because of the velocity structure. The Harvard CMT best-double-couple solution is similar in orientation, but with a much larger moment (328/89/−88/15 km (fixed)/1.8×10^{19} N m/97 per cent double-couple), probably because of the shallower depth and low surface reflection coefficients related to the sediments. This earthquake happened within the local Azerbaijan seismic network, which located it at a depth of 25 km (T. Mamedov, private communication, 2001).

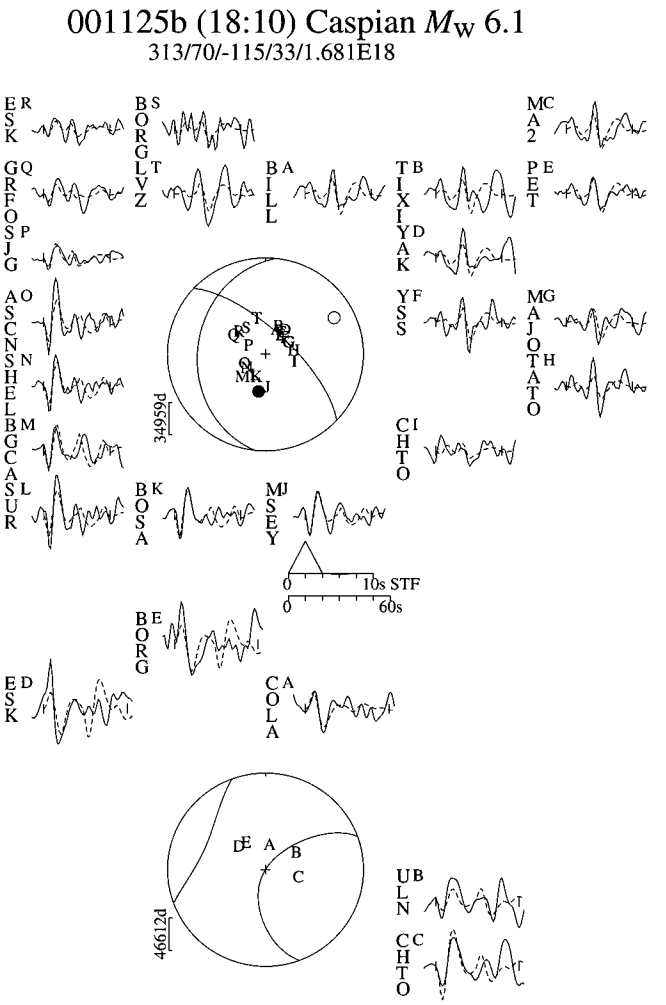

Figure A16. Minimum misfit solution for the second earthquake near Baku on 2000 November 25, at 18:10 with M_w 6.1. Synthetic seismograms were calculated with the velocity structure used in Fig. A15. This event occurred only 100 s after the first earthquake (Fig. A15) and there are fewer clear seismograms. Nonetheless, the similarity of the waveforms with those in Fig. A15 is evident. The Harvard CMT best-double-couple solution is similar in orientation and depth, but again has a larger moment (303/67/-88/26 km/6.7 × 10^{18} N m/62 per cent double-couple). The local Azerbaijan network located this event at 35 km (T. Mamedov, private communication, 2001).

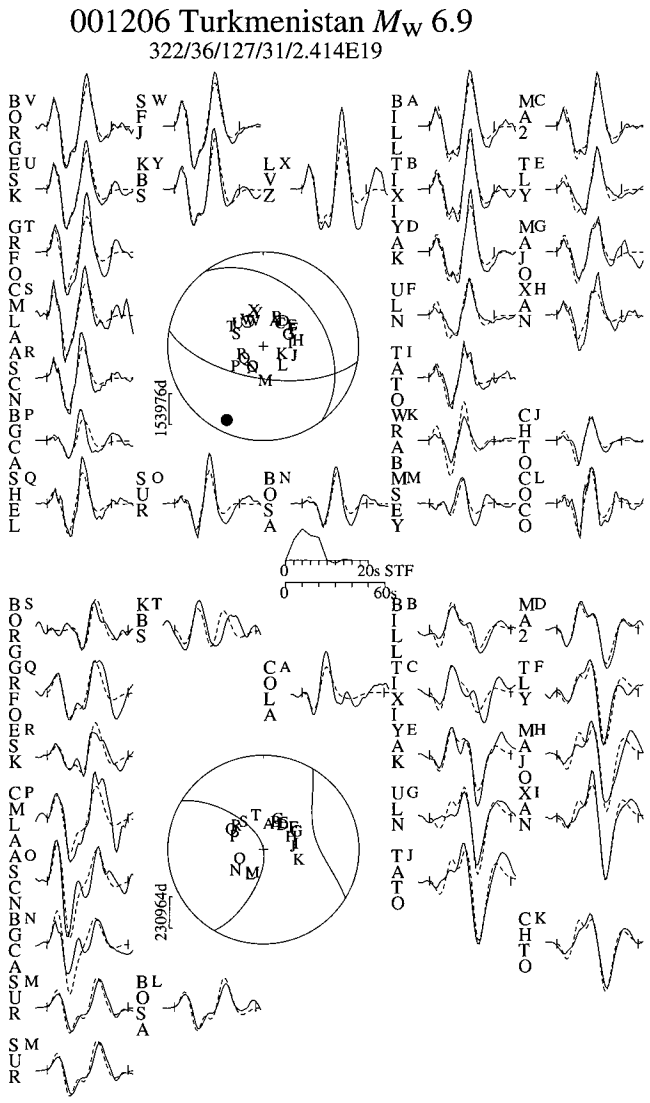

Figure A17. Minimum misfit solution for an earthquake at 31 km depth near the Balkhan in Turkmenistan on 6 December 2000 (M_w 6.9). With the large number of exceptionally clear seismograms and good reflected phases, the source parameters of this earthquake are well resolved. This is an area where the Moho is known to be at about 45 km (Mangino & Priestley 1998). We used a velocity structure in which a 20 km-thick layer with V_p=6.0 km s^{-1}, V_s=3.45 km s^{-1} and density (ρ) 2.78 Mgm m^{-3} overlaid a half-space of V_p=6.8 km s^{-1}, V_s=3.92 km s^{-1} and density (ρ) 2.91 Mgm m^{-3}. The Harvard CMT best-double-couple solution is similar in orientation (319/33/136/33 km (fixed)/3.9 × 10^{19} N m/82 per cent double-couple).

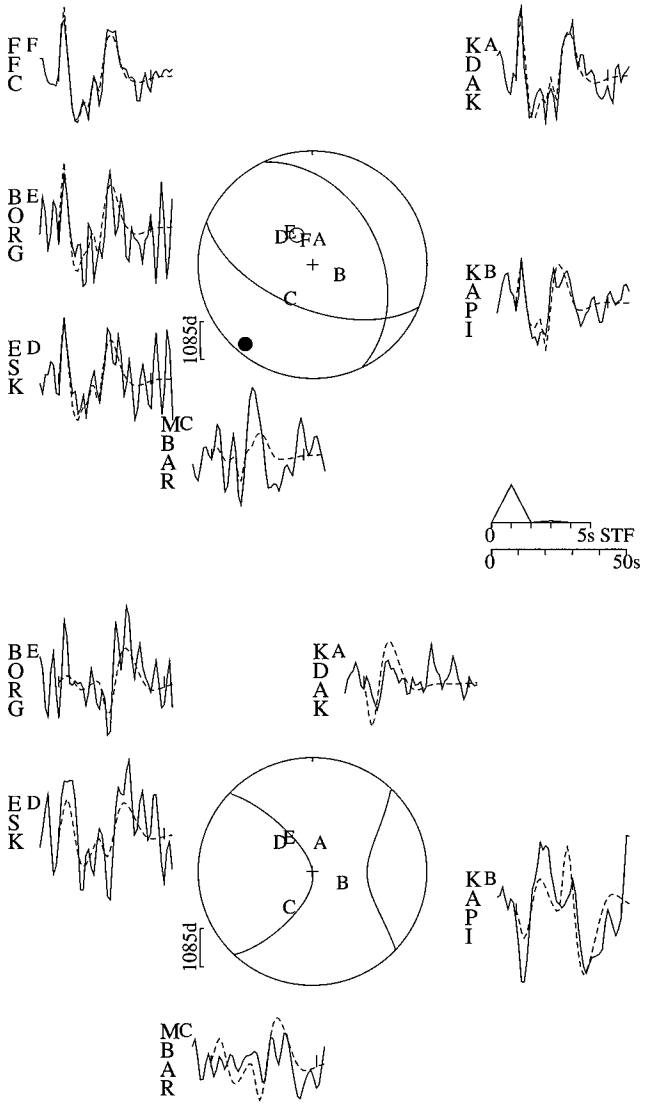

Figure A18. Minimum misfit solution for a relatively small earthquake (M_w 5.3) near the Balkhan in NW Turkmenistan on 10 June 2001. Relatively few seismograms were available, but enough to confirm that the depth of 31 km reported by the USGS Quick Moment Tensor solution was approximately correct. In the inversion we used the same velocity structure as in Fig. A17, and held the orientation at 112/58/64 (the USGS solution), inverting only for the depth, time function and moment. The preliminary Harvard CMT best-double-couple solution is similar in orientation (108/57/72/56 km/1.4 × 10^{17} N m/100 per cent double-couple), but with a greater depth.